

DESIGN AND FABRICATION OF ELECTROSTATICALLY ACTUATED AND
INKJET PRINTED MICRO-ELECTRO-MECHANICAL-SYSTEM(MEMS)
SWITCH

by

Mahmuda Akter Monne

A thesis submitted to the Graduate College of
Texas State University in partial fulfillment
of the requirements for the degree of
Master of Science
with a Major in Electrical Engineering,
August 2017

Committee Members:

Yihong Maggie Chen, Chair

Ravi Droopad

Namwon Kim

COPYRIGHT

by

Mahmuda Akter Monne

2017

FAIR USE AND AUTHOR'S PERMISSION STATEMENT

Fair Use

This work is protected by the Copyright Laws of the United States (Public Law 94-553, section 107). Consistent with fair use as defined in the Copyright Laws, brief quotations from this material are allowed with proper acknowledgment. Use of this material for financial gain without the author's express written permission is not allowed.

Duplication Permission

As the copyright holder of this work I, Mahmuda Akter Monne, authorize duplication of this work, in whole or in part, for educational or scholarly purposes only.

DEDICATION

I dedicate my thesis work to my family and friends. A special feeling of gratitude to my loving parents, Md. Siraj Uddin and Mst. Jayeda Akter whose words of encouragement and a push for tenacity ringing in my ears. My only brother Md. Jahangir, sisters Shanaj and Shamima have never left my side and are very special to me.

I also dedicate this thesis to my many friends and who have mentally supported me throughout the process. I will always appreciate everything they have done, especially Farzana Rahmat Zaki, Masudul Hassan Quraishi, Humayra Tasnim Priyanka, Ishrat Ahmed Maureen, Md.Imran Bin Azad. Special thanks also goes to one of my little friend and sister Tasnuva Uditia for the many hours of proofreading.

Finally, I dedicate my work to my best friend and my husband Mohammad Azim UI Ekram for being there for me throughout the entire master's program. He never stops encouraging and believing me all those hard times.

ACKNOWLEDGEMENTS

I would like to first acknowledge Professor Yihong Maggie Chen for her extraordinary level of support and patience. I will always remember those countless hours she spent with me in the interpreting theoretical aspects, experimental data, or just offering words of wisdom. I would also thank Professor Ravi Droopad for his encouragement, inspiration and positive thinking when I needed them the most. Thank you, Dr. Chen, and Dr. Droopad for your intellectual guidance and moral support over the past two years. I would like to also take this opportunity to thank Dr. Kim for agreeing to serve as one of the committee member of my thesis committee and for his insightful comments over the course of this thesis.

This project was supported mainly by Northrop Grumman Corporation, California and NASA John.H Glenn Research Center. I am thankful to Xing Lan and Chunbo Zhang from Northrop Grumman for intriguing discussions and the fabrication support till the final switch design.

I would like to thank my fellow lab mates and colleagues Evarestus Enuka and Mohiuddin Jewel for solving various theoretical problems and helpful group discussions.

I also would like to extend my thankfulness and abundance of love for my husband Mohammad Azim-Ul-Ekram for his candid dedication for me to achieve my goal. Thank

you for never abandoned me in my most stressed moments, without you I would have been lost somewhere. You have stayed strong and given me strength too.

I want to thank my parents for their understanding and support to let their daughter to be in thousands of miles away from home. Their love and sacrifices will not be forgotten. I can never repay what they have given to me and will make sure my future children feel the same way about me.

TABLE OF CONTENTS

	Page
ACKNOWLEDGEMENTS.....	v
LIST OF TABLES.....	x
LIST OF FIGURES	xi
ABSTRACT.....	xiii
CHAPTER	
I. INTRODUCTION	1
Introduction.....	1
Background.....	2
Printing Technology.....	3
Inkjet Printing	3
Line Patterning.....	5
Screen Printing.....	6
Flexible Materials for Printed Electronics	7
MEMS Switches	8
Other Micro Relays/Switches	9
Motivation and Goal	10
Transistor Switch Vs MEMS Switch.....	11
Quick Summary of Printed MEMS Switch	12
Thesis Overview	12
II. ELECTRICAL BREAKDOWN IN AIR GAPS	13
Introduction.....	13
Electrical Breakdown Theory: Paschen’s Law	14
Townsend Mechanism	15
Streamer Mechanism	16
III. ACTUATION THEORY OF MEMS DEVICES	18
Introduction.....	18
Piezoelectric Actuation Scheme	18
Electrostatic Actuation.....	20
Chosen Actuation Scheme: Electrostatics	21

Pull-down or Actuation Voltage	22
Release Voltage	23
IV. DEVICE FABRICATION PROCESS.....	24
Introduction.....	24
Fujifilm Dimatix Materials Printer	24
Effect of Cartridge Angle on the Printing Resolution	25
Droplet Formation by MEMS Technology.....	27
Device Fabrication by Inkjet Printing.....	29
Flexible Electronics Fabrication by Printing Process	29
Resolution Limit	30
Material Evaluation.....	31
MEMS Switch Fabrication	37
Schematic of Fabrication Steps of Typical MEMS Switch	37
Creating Design File	40
First Complete Printed MEMS Switch	41
V. DEVICE TESTING AND DC ANALYSIS	44
Introduction.....	44
Instrumentation (Software and Hardware).....	44
KLA-Tencor.....	45
Apex Software	45
4-Point Probe Resistance Measurement.....	46
Device Characterization.....	46
Test Device: 1	46
Material Selection and Evaluation	47
First Fully Printed MEMS Switch	48
First Tested MEMS Switch.....	48
Sacrificial Layer Deposition and Etching.....	49
Releasing Membrane	50
First Successful Device (Fabrication and Testing)	52
Analysis of Bottom PEDOT Layer	53
Analysis of Ag Sacrificial Layer.....	54
Analysis of Complete Device Before Etching.....	55
Resistance Measurement of the Device Before Etching.....	56
Etching of Ag Sacrificial Layer	57
Resistance Measurement of the Device After Etching	57
Thickness Comparison Before and After Etching	58
MEMS Switch Testing: DC Performance Analysis.....	60
Experimental Results	61

Calculated Actuation Voltage	63
VI. CONCLUSION AND FUTURE WORK	65
Introduction.....	65
Summary.....	65
Conclusions.....	66
Recommendations for Future Work.....	67
APPENDIX SECTION.....	69
REFERENCES	72

LIST OF TABLES

Table	Page
1. Commercially available polymers for printed electronics	8
2. Specification requirements of switching devices.....	9
3. Comparison among transistor switches and MEMS switches	11
4. An upfront summary of the performance of the fabricated MEMS switch	12
5. Typical properties of PEDOT [45]	31
6. Evaluation for silver ink.....	35
7. Designed critical thickness of each layer.....	40
8. Final thickness and width of each layers of printed switch	42
9. Set parameters during the printing of each type of material ink printing	43
10. Material evaluation for very first fabricated device on silicon substrate.....	47
11. Measured resistance before etching.....	57
12. Measured resistance after etching.....	58
13. Data table for input voltage and output current for connection type 1	62
14. Calculated actuation voltage by considering air gap between electrodes.....	64

LIST OF FIGURES

Figure	Page
1. Drop formation by a thermal inkjet printer.....	4
2. Design of a (a) shear mode (b) bend mode piezoelectric inkjet print head	5
3. Structure of line patterned field effect transistor	5
4. Typical Paschen curves for hydrogen and air	14
5. V-I plot of two parallel plates	16
6. Electrostatic actuation scheme [31]	20
7. Fujifilm Dimatix material printer system	25
8. Print carriage or printer head system	26
9. Relationship of cartridge angle versus material deposition	27
10. Formation of a droplet in the nozzle [41]	29
11. Surface treatment effect on PEDOT printing.....	32
12. Typical RIE chamber for oxygen plasma treatment while plasma treatment.....	33
13. High temperature curing effect on PEDOT printing.....	36
14. Switch process flow.	37
15. Schematic of fabricated MEMS switch	39
16. Layer by layer design file created by AutoCAD 2017	41
17. All three layers of device and cantilever.....	42
18. Top and side view of modeled MEMS switch.....	46

19. Schematic of printed MEMS switch.....	48
20. (a) First printed layer by Ag ink (b) First and second layer (Ag and PEDOT)	49
21. 2D analysis of the Cu sacrificial layer	49
22. Complete device on silicon substrate with Cu sacrificial layer	50
23. Cu etching test.....	52
24. Printed PEDOT layer test.....	54
25. Printed sacrificial layer test.....	55
26. Testing of complete three-layer device.....	56
27. Device testing before and after etching	57
28. Thickness comparison after etching.....	59
29. Thickness comparison in anchor region	60
30. Two different types of connection for device testing	61
31. Input voltage vs output current for connection type 1	63
32. AutoCAD design for 2×2 phased array antenna.	68

ABSTRACT

This thesis report presents the design and fabrication process of electrostatically actuated and inkjet printed MEMS switch. It introduces a novel design and fabrication process where it combines two different technologies - MEMS technology and inkjet printing technology. It should also to be noted that, for the first-time inkjet printing technology is introduced for the fabrication of a MEMS device. The physical structure of the switching system consists of an anchor, the cantilever beam, top electrode and bottom transmission lines. During the fabrication process, different printed layers are characterized with respect to terminal resistances, sheet resistances of the materials, critical thickness of each layer, conductivity etc. Finally, after DC analysis of the fully printed switch, 1.2 V is found to be the minimum achievable pull-down voltage for the electrically actuated cantilever beam. The air gap between the top and bottom electrodes were in micron-scale during DC analysis. At the end of the thesis, the experimental data are compared with the theoretical data. It is found that, the experimental data is closely correlated with the theoretical assumption.

I. INTRODUCTION

Introduction

In near future, a highly realistic and innovative integration of three technological areas - microelectronics, chemistry and printing is foreseen that will create markets with annual revenues estimated at more than \$200 billion [1]. Inorganic semiconductors such as silicon, germanium and gallium arsenide have been widely used in semiconductor industries for more than last four decades [1]. Silicon dioxide insulators and metals such as aluminum and copper are the backbones of printed and flexible electronic technology. The combination of conductive polymers and inorganic materials with printing technologies enables thin, lightweight and extremely cost-efficient electronic systems. Current market drivers are organic photovoltaics [2], flexible batteries [3], [4], electro-optic devices [5], [6] displays, logic and memory components including field effect transistors (FETs) and thin film transistors (TFTs) [7], sensor arrays [8], [9], and radio frequency identification (RFID) tags [10]. However, solution processable semiconductors and metals are fast replacing traditional inorganic materials due to their numerous advantages. Most important advantages of solution processable materials include ease of device fabrication, compatibility with light weight, mechanically flexible base materials and easy control of electrical, optical and magnetic properties [11]. Solution processable materials are usually organic based and the branch of electronics that deals with these materials is called plastic electronics. It is also referred to as “flexible electronics”. The area of flexible electronics builds functional devices on mechanically flexible substrates that uses solution processable organic, inorganic and hybrid materials.

This thesis presents a complete design and fabrication process of a MEMS switch where basically three different research areas has been combined such as printed electronics, flexible electronics and MEMS technology. Printing technology (inkjet printing) is used to fabricate the MEMS switch on flexible substrate. This switch is normally an open, single port single through switch. The prototype of this switch employs a vertically moving cantilever beam structure, between a top and bottom electrode. In addition to the physical structure, the application of the switch is also investigated. At the end, the performance results and characteristic parameters are used as general design guidelines for the printed MEMS switch. The design theories are comprehended through fabricated switches with good agreement between the theory and the experimental data. Our design of a MEMS switch employs a few stacks of printed structure with a clamped rectangular cantilever as the moving structure.

The following sections contain the historic background of printing technology, flexible materials, other micro switching devices, the device attributes, and applications. Later, a brief description of the project motivation and goal is described. Finally, the framework structure of the thesis is outlined.

Background

Inkjet printing techniques have been gaining attention because of their simplicity of fabrication, compatibility with different substrates, low temperature processing, feasibility of non-contact and mask free patterning and low cost [11]. It is a common method used in nearly every office and household to transfer computer data to paper or transparencies. The same technology with simple modifications is used to print conductive patterns by nanoparticle conductive inks on various substrates including glass, semiconductor

materials, overhead transparencies and even paper [12]. It is also possible to achieve layer by layer printing with different thickness and different structures in every layer, which is why it is also referred to as 3D inkjet printing technique.

Printing Technology

The attraction of printing technology for the fabrication process is greatly influenced by the ease of the fabrication process. Also, the easiest fabrication process on mechanically flexible materials plays a very important role. It is possible to achieve multilayered microstructures and thin-film devices in a much simpler and cost-effective way [12].

The most widely used printing techniques are inkjet sheet-based or screen printing, offsets and flexographic and gravure printing [12]. Sheet-based inkjet or screen printing is generally used where low-volume, high-precision work is required. To produce high volume inorganic and organic conductors, offset and flexographic printing are more commonly used. Gravure printing has a high layer quality, and is especially suitable for quality-sensitive layers such as organic semiconductors and semiconductor/dielectric-interfaces in transistors. Organic field-effect transistors (FETs) and integrated circuits (ICs) can be prepared batch by batch completely by mass-printing methods.

Inkjet Printing

Inkjet printers can be divided into two basic groups based on their operation procedure-continuous and drop-on-demand [12]. In continuous inkjet printers, the ink is first pumped through a nozzle forming a liquid jet. Secondly, the formed liquid jet is deflected by electrostatic plates to the paper or to a reservoir for recirculation.

Today most inkjet printers are based on the drop formation process, which is called drop-on-demand (DOD) [11], [12]. The drop-on-demand method provides smaller drops

and higher placement accuracy compared to the continuous inkjet printers. In this method, pulse that creates the ink drop can be generated either thermally or piezoelectrically. As seen in fig. 1, in a thermal inkjet printer a heated plate causes a vapor bubble, which pushes the ink out through the nozzle. The total ejection time is a few microseconds and the temperature of the plate can rise by about 300 °C during the ejection.

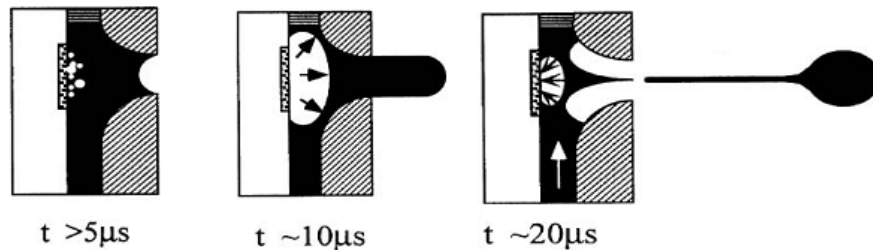


Figure 1. Drop formation by a thermal inkjet printer. (The Society for Imaging Science and Technology sole copyright owners of The Journal of Imaging Science and Technology) [13]

Piezo-ceramic tubes, rods, or plates is used in the cartridge head of piezoelectric inkjet printers. Fig. 2 (a), shows a schematic of a shear mode piezoelectric print head. In this type of print head, an electric field applied to a piezo-ceramic actuator element causes shear action deformation and that is used to eject the ink through the nozzle [7]. The print head design shown in fig. 2 (b), is called the bend-mode design. In this design, ink rejection is caused by the piezo-ceramic plates bonded to a diaphragm to form an array of bilaminar electromechanical transducers.

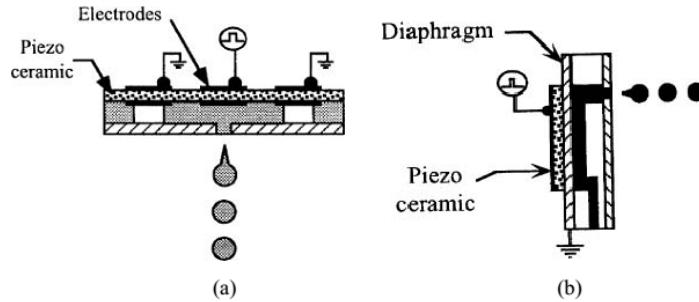


Figure 2. Design of a (a) shear mode (b) bend mode piezoelectric inkjet print head (The Society of Imaging Science and Technology sole copyright) [13]

The print heads in a Tetronix's Phaser 300 and 350 and Epson's Color Stylus 400, 600, and 800 inkjet printers are of the bend mode piezo-ceramic type.

Line Patterning

Among all printing methods, line patterning is the simplest and the cheapest method, introduced by MacDiarmid and coworkers [14]. This method includes, (i) the design of a negative image of the required pattern using a computer aided design software, (ii) deposition of a conductive polymer on the substrate, and (iii) removing the printed mask by sonicating the substrate in toluene for ~10s. Line patterning methods can be used to fabricate resistors, RC filters, FETs (fig. 3), RF identification tags etc.

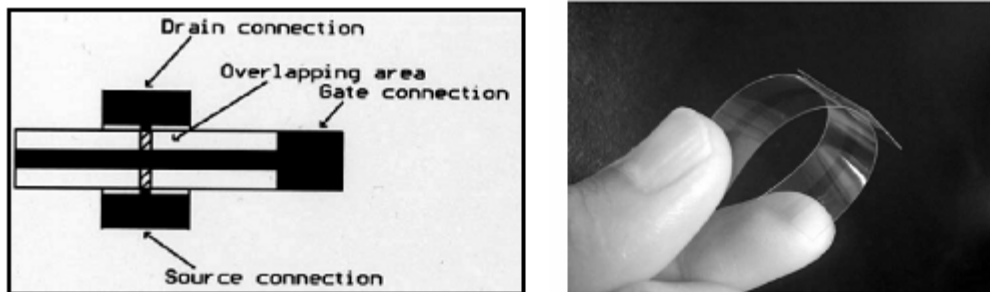


Figure 3. Structure of line patterned field effect transistor [15].

MacDiarmid et al. fabricated FETs on overhead transparency substrates by using PEDOT/PSS as the active material and UV curable epoxy as the insulating material between the source-drain and gate electrodes [16]. When a positive voltage is applied to

the gate electrode, electrons are induced into the channel at the interface between the insulator and PEDOT/PSS layer due to a capacitance effect [16]. The flow of induced electrons from the source to drain is controlled by the gate voltage by affecting the size and shape of a conductive channel. This conductive channel is the path through which electrons flow from source to drain [17].

Other methods with similarities to printing are micro contact printing and nano-imprint lithography. In these methods, μm - and nm -sized layers are prepared by methods like stamping with soft and hard forms respectively. Often the actual structures are prepared by subtractive method, e.g. by deposition of etch masks or by lift-off processes.

Screen Printing

Screen printing is a simple and environmental friendly printing process for depositing ceramic and polymer inks [6]. In general, screen printing is used to manufacture conductive interconnections between electronic components on circuit boards. This method involves moving a squeegee blade across a screen mesh. The squeegee blade pushes ink through a screen mesh, which is patterned by means of a stencil, to produce open areas which result in a conductive material pattern on the circuit board. This method is compatible with high viscosity materials including conductive inks, dielectric pastes, UV curable materials and various adhesives. Bao et al. [8] fabricated organic FETs using screen printing technology. They used a screen mask made of a stainless-steel fabric with 400 mesh/count to deposit an insulating polymer layer (polyimide) and a source-drain electrode (conductive ink 479SS from Acheson Co.). Knobloch et al. [9] also manufactured organic FETs by screen printing a semiconductor active layer of poly(3-alkylthiophene). Screen printed inductors

[10] , biosensors [11], [12], solar cells [13], [14], gas sensors [15], [16], and strain sensors [18] have been reported.

Flexible Materials for Printed Electronics

Polymeric material is used in most flexible electronics and/or organic electronics application. A polymeric solid is made of many repeating chemical units or molecules called monomers. Polymers can exhibit various mechanical, electrical and optical properties depending on the synthesis conditions and chemical properties. The electrical conductivity of insulating polymers is about 10^{-18} S/m whereas that of doped trans-polyacetylene is 107 S/m [19]. Some polymers such as, poly (cis-1,4-isoprene) and poly(chloromethylstyrene) are sensitive to high-energy radiation. If the polymer is exposed to ultraviolet light, the chemical properties, such as solubility of the polymer in the exposed area change. Photolithography is a very well-known process in electronics that uses this principle.

To understand the electronic properties of polymers, it can be considered that every repeated unit is a separate molecule having molecular orbitals in a certain electronic state [4]. Therefore, the number of repeat units determines the electronic properties of the polymer.

Table 1. Commercially available polymers for printed electronics

Name	Specifications	Properties/Current Limits
Riston® (DuPont) [31]	Dry Film	A “General Purpose” dry film for acid and alkaline etch up to 15 μm
Kapton® (DuPont)	Dry Film	A “General Purpose” dry film for printing with all types of Nanoparticle ink (Ag, Au, CNT)
Novacentric Novela® (NOVELA Advance Microsystem)	One sided dry film.	Substrate thickness: 10-25 μm (0.4-1mil) Minimum track width and spacing: 10 μm (0.4mil) Minimum dielectric layer thickness: 1.8 μm (0.07mil)

MEMS Switches

MEMS is an advance technology that allows device fabrication at a submillimeter scale for different components. Currently a large variety of MEMS devices such as sensors, actuators and switches are available. Currently these devices are developed and fabricated by cleanroom micromachining technology. In this thesis, recently developed inkjet printing technology has been introduced to develop and fabricate MEMS devices on top of a flexible substrate. A high frequency MEMS switch could provide switching capability at radio frequency (RF) or even microwave frequencies. These switches extend several advantages that make them an alluring alternative to conventional devices like mechanical relays and solid-state devices. MEMS also can provide low insertion loss, high isolation, low power consumption, extreme linearity and the ability to be integrated with other electronics.

There are also some other switching devices. They usually have three terminals where one of the terminal is the control terminal, other one is the line terminal and finally merged

into one by creating the third terminal. Terminal one and two share common electrical potential. *Audion* or triode was the first *electronic* switch invented back in the early twentieth century [20]. Audions were also called *grid-controlled* vacuum-tube rectifiers. The invention of such rectifiers marked the dawn of the vacuum tube era which spanned over the first half of the twentieth century. Basic semiconductor power switching devices include diodes (bipolar and Schottky), transistors, MOSFET, and thyristors are invented in the early 1940-50's [21], [22]. The achievement of microelectronics is empowered by the improvement of semiconductor fabrication technologies. These technologies are continually making it possible to invent smaller and better devices.

Different applications required different types of switching devices. The two most widely used applications of switching devices are signal routing and power routing. These two types of switches have common requirements, such as long lifecycle, robust operation, high open-contact and control-to contact breakdown voltages, minimal bouncing effects etc. Table 2 Illustrates the common features of signal MEMS switch and power MEMS switch.

Table 2. Specification requirements of switching devices: Signal switching vs. Power switching

Signal MEMS Switch	Power MEMS Switch
Signal switching (High-fidelity)	Power switching (High-efficiency)
Low insertion loss	Low on-state voltage drop
Wide frequency bandwidth	High current capacity
Low signal cross-talk	Low off-state leakage current
Low parasitic impedance	---

Other Micro Relays/Switches

The development of MEMS switches has gained global attention. Scientists are trying to look for the possibility of merging conventional macroscopic relay attributes with MEMS

device attributes to develop a new family of switching devices: MEMS based relays/switches. One of the earliest MEMS devices developed two decades ago, was an electrostatic switch [23]. An electrostatic based actuation remains the most popular actuation scheme, but other methods such as electrothermal actuation, magneto static actuation and piezoelectric actuation have also been broadly investigated.

From the literature study it is found that, most of the MEMS relays/switches are focused on signal switching applications, such as automatic test equipment [24], [25], telecommunications [26], [27], and logic operation [28]. On the other hand, only few MEMS based switches are found to be for power applications [29].

Motivation and Goal

Cleanroom micromachining/photolithography is most widely used technique for design and fabrication of MEMS switches. Even though this technique has lots of advantages, it still has some inherent problems as follows [30]:

- I. Complexity of design procedure
- II. Time lengthy process of device fabrication
- III. Reliability issues
- IV. Costly manufacturing process

Printed MEMS switch may empower potentially new and large markets in printed and flexible electronics research area. In this thesis, the inkjet printed MEMS switch has been developed on Du Pont kapton polyamide substrate. This flexible substrate has the advantage of providing low-cost and disposable device fabrication. Fabrication using inkjet printing technology has lower manufacturing cost, does not require vacuum, roll-to-roll

and large-area processing. Moreover, inkjet printing also possesses advantages as in the case of contact-less fabrication onto fragile substrates.

The objective of this thesis is to overcome the challenges of cleanroom micromachining/photolithography technique for MEMS technology. Also, the fabrication of this MEMS switch is prominent due to its wide range of application in reconfigurable antennas such as phased array antenna, microstrip antenna, dipole antenna, slot antenna etc. These switches can offer very low actuation voltage with high on/off ration, low loss switching and can be controlled by (10-120) K Ω resistive transmission lines. The printed MEMS switch fabricated in this thesis will be used as a signal switch.

Transistor Switch Vs MEMS Switch

Table 3 shows the comparison among transistor switch and MEMS switch. In this it is seen that the actuation or turn-on voltage is high for typical MEMS switches but the performance in high frequency application is better than transistor switches.

Table 3. Comparison among transistor switches and MEMS switches

Parameters	PIN Diode Switch	FET Switch	MEMS Switch
Actuation Voltage (V)	$\pm 3 - 5$	3 - 5	20 – 80
Actuation Current (mA)	3 - 20	0	0
Power Consumption (mW)	5 - 100	0.05 – 0.1	0.05 – 0.1
Switching Time (μ s)	0.01 – 0.1	0.001 – 0.1	1 – 300
RF Isolation (1-10 GHz) (dB)	35	15 - 25	40
RF Isolation (> 10 GHz) (dB)	20 - 35	20	25 – 40
Insertion Loss (1-10 GHz) (dB)	0.3 – 0.7	0.4 - 2	0.05 – 0.2
Insertion Loss (> 10 GHz) (dB)	0.7 - 2	2	0.1 – 0.2

Quick Summary of Printed MEMS Switch

To put the inkjet printed MEMS switch in perspective with other micro switches, this section tabulates basic parameters of electrostatic actuated MEMS switches in Table 4.

Table 4. An upfront summary of the performance of the fabricated MEMS switch

Actuation Scheme	Electrostatic
Actuation Voltage	1.2 V
R (Cantilever-Transmission Line), Connected by sacrificial Layer	(280~400) Ω
R (Cantilever-Transmission Line), After removal of sacrificial Layer	(2.5~3.0) M Ω
R (Transmission Line-Transmission Line), Connected by sacrificial Layer	(380~450) Ω
R (Transmission Line-Transmission Line), After removal of sacrificial Layer	(0.40~0.55) M Ω
Current Capacity	(0.0068~0.2195) mA
Current ON-OFF ratio	68:1

Thesis Overview

This thesis is organized in a total of six chapters. The current chapter is an introduction which begins with background study of printing technology, flexible electronics, MEMS switches and other micro switches. Finally, this chapter ends with the motivation and goals of the thesis and the summary of the prototype device performance. Chapter II investigates the theories of electrical breakdown in narrow air gaps; this theoretical study establishes guidelines for the future MEMS switch design. Chapter III analyzes different actuation schemes. This chapter also briefly describes the electrostatic actuation and why this scheme was chosen in our current research. Chapter IV focuses on the device fabrication by inkjet printing techniques. Chapter V discusses device testing, characterization and dc analysis; also, how the tests are implemented, and their results. Finally, a summary, conclusions, and suggestions for future works are given in Chapter VI.

II. ELECTRICAL BREAKDOWN IN AIR GAPS

Introduction

This chapter focuses on two main theories of MEMS to work as a switching device. First, the physical property of electrical breakdown phenomena in micron scale air gaps. Second, observational study of achievable actuation and standoff voltage in such narrow air gaps. Electrical breakdown in narrow air gap is the first challenge of this thesis. Because of that, experimentation of the electrical breakdown test is one of the most important step toward actual MEMS switch fabrication.

To achieve an in-depth knowledge of electrical breakdown in narrow air gap, it is necessary to consider different influential factors for electrical breakdown. The factors include gap spacing between electrodes, electrode surface condition, electrode shape, materials of electrode, air pressure, air temperature and uniformity of electrical field [31]. There are also very fundamental factors that can affect the break down process such as atomic, molecular, electronic, ionic, and photon collision process in the air [31]. A full-scale study of these fundamental factors can make up a doctoral thesis in elementary physics, and it is not viable to carry out these phenomena here. In this this, the effect of two most important parameters; air gap separation and the physical structure of cantilever beam will be investigated.

This chapter develops a key understanding of the electrical breakdown in narrow air gaps and some existing theories of electrical breakdown which are found in literature.

Electrical Breakdown Theory: Paschen's Law

There are different factors that should be considered in studying the breakdown in air as well as gases, temperature, pressure, surface condition, the shape of electrode, material of electrodes and the gap spacing between electrodes. In 1889 Paschen found an empirical criterion [32] as follows: the breakdown voltage of air/gas depends on gas pressure and gap separation. The dependency relation is a product of gas pressure and gap separation when pressure and temperature is over a certain range in the static uniform field. Mathematically it can be represented as follows [32],

$$V_s = f(pd) \quad (1)$$

where V_s is the breakdown voltage, p is the gas pressure at a known temperature, d is the gap separation, and f is a function of pd . This criterion is applicable for a pressure of about 150 psi and it's known as Paschen's Law [32].

Fig. 4 shows Paschen's curve for hydrogen and air. From the curve, it is seen that, the breakdown voltages for air/gases decrease as the product of gas pressure, p and gap separation, d is reduced, and reach a minimum at a value of their product as pd on the order of 1 to 10mm-Hg \times cm [33], [34].

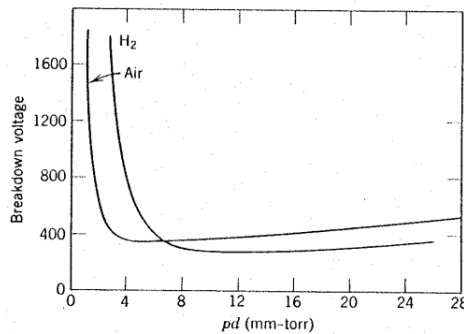


Figure 4. Typical Paschen curves for hydrogen and air [35]

Nowadays, two fundamental breakdown mechanisms have been established namely Townsend mechanism and Streamer mechanism [31]. Townsend mechanism is relatively slow; it needs many electron generations to produce breakdown. This is also referred to as the Generation Mechanism. The Streamer mechanism is a rapid mechanism; it develops directly from the first avalanche to breakdown. This is also referred to as the Kanalaufbau mechanism [31]. These two mechanisms are briefly discussed next.

Townsend Mechanism

In 1910, the Townsend's theory, was illustrated [36] by examining the current between parallel plate electrodes increasing electric force; see fig. 5. At first, the leakage current between the plates increases with electric field. This leakage current also saturates very quickly at a certain value, I_0 . After that, a wide range of electric potential change does not affect the leakage current much. Finally, the rate of leakage current increase suddenly to an appreciable value at some higher potential. Townsend explains this phenomenon as "Under low electric field, a dielectric gas is in its normal state and electrically non-conductive because there is no significant number of free electrons or ions to carry electrical current between the electrodes [31]. However, there is always a small number of low energy charged particles present in the gas due to environmental radioactivity and cosmic radiation" [36].

At low electric field, a limited number of free electrons are responsible for the leakage current, I_0 . A single free electron could produce two free electrons and a positive ion by collision. Ions will generate more charged particles for more electron collision due to higher electric field intensity. This accumulation of electrons eventually produces a crowd of free electrons and ions, generally called "electron avalanche" [31]. After this

electron avalanche process, the gas becomes conductive. Furthermore, because of the continuous avalanche of positive ions, a secondary avalanche may occur at the cathode. This creates a self-sustaining discharge or electrical breakdown. This model is commonly known as the Townsend theory of breakdown [36].

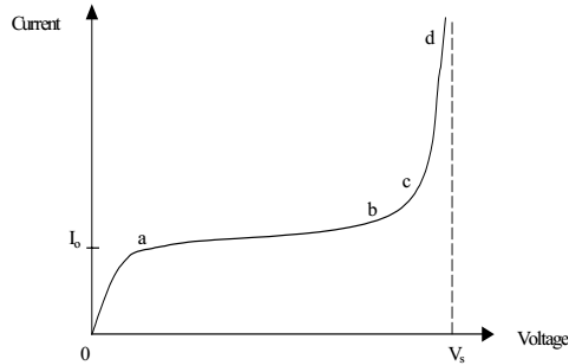


Figure 5. V-I plot of two parallel plates (Townsend electrical breakdown mechanism) [36]

Streamer Mechanism

This section describes another breakdown mechanism which is much faster than the Townsend Mechanism [31]. The most important features of this mechanism are as follows:

1. The breakdown potential of this mechanism is independent of the nature of the cathode surface as there is no cathode secondary ionization. Additionally, free electrons produced by photons from the avalanche head by photo-ionization [37].
2. Free electrons move toward the avalanche head and generate cumulative avalanche, because of high field distortion and space charge at the avalanche head. Breakdown occurs as soon as the space charge distorts the field. Finally,

breakdown potential is uniquely determined by space-charge distortion of the electric field [37].

3. It is possible that breakdown can take place within less than $0.1 \mu\text{s}$ for a 1 cm gap, and that luminous streamers can also cross the gap by taking less than an electron transit time [37].

The Streamer theory is applicable only when the number of electrons in the average avalanche reaches to a critical value which is commonly 10^8 [31]. The Townsend mechanism operates at the lower pd values where the transition from this mechanism to a Streamer mechanism takes place when $pd > 200$ torr-cm, where p is the gas pressure between the parallel plate electrodes and d their gap separation distance [31]. In traditional relays or MEMS switches, the contact separation ranges from millimeters down to micrometers when its open. Therefore, the Townsend mechanism works better than the Streamer mechanism for small air gap [31].

III. ACTUATION THEORY OF MEMS DEVICES

Introduction

According to some experts, combining science and art in the most effective and creative ways can lead to the best designs. Design practice resembles sophisticated art that requires perception for perfection and efficiency. An axiomatic design approach always exists for the designer to follow in well-established domains [31]. However, many MEMS device design problems are backed with a somewhat limited knowledge base, and becoming an ad hoc activity with necessary trial-and-error process. Even with a constant problem statement, in some cases the thesis objective is a continually moving target since discoveries of limitations and possibilities in MEMS technologies are still being constantly learned.

This chapter is an effort to shed some lights to the decision-making process of designing MEMS switches to avoid at least some of the unacceptable designs. This is also a contribution to the knowledge base of MEMS design so that the designing process can be packed with more facts and less trial-and-error.

The theories used in the design of the MEMS power switch is discussed in this chapter, that includes, actuation schemes commonly seen in MEMS devices and the reason for selection of an electrostatic scheme is explained.

Piezoelectric Actuation Scheme

When an electric field is applied to piezoelectric materials, they tend to deform, or conversely, generate an electric field under the action of an applied strain. This strain, ϵ , under the action of an applied electric field is given by [31]:

$$\varepsilon = \sigma s + Ed \quad (2)$$

Where, ε is the strain in the piezoelectric material, σ is the applied stress, s is the elastic compliance constant, E is the electric field, and d is the piezoelectric strain constant. For typical materials, the piezoelectric strain coefficients, d_{ij} , are very small values, typically on the order of 1 to 3 Å/Volt, resulting in very small displacements. For considerable amount of displacements, increasing the physical size of the piezoelectric actuator, or using a displacement amplifier is desirable [31]. Although, the former is incompatible with the goal of miniaturization and the latter is achieved at the price of a small actuation force. Typical displacement values for macro-scale piezoelectric actuators of a few centimeters in length are 250 ~ 500 Å/Vol [31]. The piezoelectricity generates a reasonable amount of force if the sample can be held at zero strain. But as the material expands the force declines. This is evident from the equation below [31]:

$$\sigma = P = \frac{1}{s}(\varepsilon - Ed) \quad (3)$$

Where, P is the pressure of reaction applied by the material to its environment. Apparently, from Equation (3.2), the maximum pressure can only be achieved by having zero strain. This property makes it not feasible to realize both large actuation and large displacement at the same time. Furthermore, the material properties itself poses a limit to the amount of achievable deformations unless large sized piezoelectric actuators are used, which negates the goal of device miniaturization [31]. To summarize, piezoelectric mechanisms generates reasonable amount of force but cannot provide enough displacement without using actuator due to limitations of material properties.

Electrostatic Actuation

Fig. 6 shows the most common micro-actuation scheme named electrostatic actuation. When an electric field is applied between two parallel plates, an attractive force is generated which acts on both plates to bring them closer and minimize the electrical potential energy of the system.

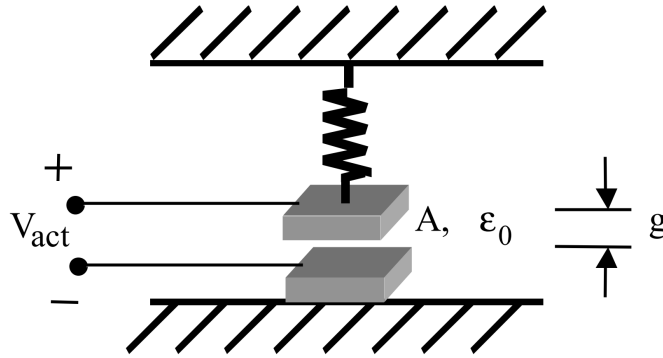


Figure 6. Electrostatic actuation scheme [31]

This electrostatic force can be written as [31]

$$f_{electrostatic} = \frac{\partial U}{\partial g} \quad (4.1)$$

$$U_e = \frac{1}{2} CV^2 = \frac{\epsilon_0 AV^2}{2g} \quad (4.2)$$

$$\text{hence, } f_{electrostatic} = \frac{\epsilon_0 AV^2}{2g^2} \quad (4.3)$$

Where U_e is the electrical energy in the system, C is the capacitance of the parallel plates, A is the cross sectional area, g is the gap separation distance between the plates, ϵ_0 is the dielectric constant of air ($8.854 \times 10^{-12} \frac{F}{m}$), and V is the potential difference across the plates [31].

Therefore, the electrostatic stress between two capacitor plates insulated by air, is given by

$$P_{electrostatic} = \frac{f_{electrostatic}}{A} = \frac{1}{2} \epsilon_0 E^2 \quad (5)$$

where E is the electrical field and $\frac{V}{g}$. Here fringing effects on the periphery is neglected. The maximum electric field for micrometer sized air-gaps before breakdown is approximately $10^8 V/m$. From equation 3.6 the calculated electrostatic pressure is limited to about $44 kPa$ ($\approx 6.5 psi$ or $0.44 atm$) [31]. Furthermore, as noted in equation 3.5, for a fixed voltage, the electrostatic pressure and by extension the electrostatic force is inversely dependent on the squared of the distance between the capacitor plates. This means that as the plates get farther apart, the electrostatic force drops quadratically. Additionally, this force is also linearly proportional to the area of plate. Hereafter, requirement of a large area with a small gap separation to generate force of significant magnitude imposes fabrication difficulties. Finally, the travel of the movable plate should not be larger than one third of the air gap, otherwise there will be a snap-through motion due to the unstable nature of the electrostatic actuation. Releasing the movable plate from electrostatic seizure requires the applied voltage to be reduced well below the voltage at which such snap-through motion occurs. This hysteresis can be avoided by restricting the displacement of the movable plate to within $\frac{g}{3}$. However, if a high actuation force is desirable in the MEMS switch operation, the hysteresis snap-through motion can be useful.

Chosen Actuation Scheme: Electrostatics

Our choice of actuation mechanism for the inkjet printed MEMS switch is electrostatic actuation of a movable cantilever beam. It can also be used in pressure control applications that require pressure switches. Tunable threshold pressure is controlled by a voltage bias. The design geometries and materials chosen for the MEMS switch are such that the

cantilever, under a small deflection, has a linear relationship between the air gap and pull-down voltage.

Pull-down or Actuation Voltage

Considering a spring-mass system with lumped parallel-plate as shown in fig. 6. when the applied voltage is under a certain threshold, an electrostatic force attracts the electrodes closer to the ground. The displacement-induced mechanical restoring force balances the electrostatic force during this time. Thus, a system equilibrium is reached when the two forces equate. However, different variables determine the electrostatic and mechanical forces on the displacement of the electrodes. There is a threshold to the applied voltage, if exceeded, causes a disparity in the mechanical and electrostatic force balance. The electrode imposes a positive force gradient and thus accelerates away from that equilibrium point. This threshold voltage is called the pull-down or actuation voltage [38].

As discussed earlier, if the gap separation is larger than one third of the actuation gap, that MEMS switch still be unstable but electrostatically turned ON, which may be preferred for contact force situation. A closed-form expression for the pull-down voltage ($V_{pull-down}$) in the case of a cantilever beam [39] is:

$$V_{pull-down} = \sqrt{\frac{\gamma_1 \sigma_0 E t g_0^3}{(1 - v^2) \epsilon_0 a^2 f(\gamma_2, k, a)}} \quad (6)$$

Where g_0 is the actuation gap separation, ϵ_0 is permittivity of air, $\gamma_1 = 1.55$, $\gamma_2 = 1.65$,

$$k = \sqrt{12(1 - v^2)/Et^2\sigma_0^2} \text{ and } f(\gamma_2, k, a) = 1 + 2 \left[1 - \cosh\left(\frac{\gamma_2 ka}{2}\right) \right] /$$

$\left(\frac{\gamma_2 ka}{2}\right) \sinh\left(\frac{\gamma_2 ka}{2}\right)$. Equation (6) can be approximated below by considering the

diaphragm mechanics is to be dominated by stress as,

$$V_{pull-down} = \sqrt{\frac{\gamma_1 \sigma_0 E t g_0^3}{\epsilon_0 a^2}} \quad (7)$$

Due to the hysteretic nature of electrostatic actuation, the actuation voltage must drop below a voltage significantly less than $V_{pull-down}$ to switch off electrostatically.

Release Voltage

Electrostatic pull-in and release take place in a snap-through action. This is because both pull-in and release correspond to the transition between stable and unstable equilibrium solutions of the force-balancing equations of Newton's first law. However, unlike electrostatic pull-in, no closed-form approximation or measurement equation is available for electrostatic release voltage of distributed mechanical systems. Using finite element analysis software capable of analyzing coupled electromechanical systems, it is possible to numerically obtain the electrostatic release voltage [40].

In this chapter two most important actuation schemes are discussed such as piezoelectric actuation and electrostatic actuation. As our MEMS device operation is based on electrostatic actuation, a brief description of this scheme is given. Finally, chapter is closed by describing the reason behind choosing electrostatic actuation scheme.

IV. DEVICE FABRICATION PROCESS

Introduction

Inkjet printing is a contactless printing technology developed in the late 1970s. The droplets of ink are jetted from a small aperture directly to a specified position to create an image.

Due to its contactless and simple additive deposition technique, it is considered a cost-effective method to produce printed and flexible electronics. This deposition method deposits materials only when needed, and it also does not require sacrificial resist or liftoff layers any time before or after deposition.

Fujifilm Dimatix Materials Printer

A Fujifilm Dimatix Materials Printer (Model: DMP-2800 series), as shown in fig. 7 (a) and a piezoelectric printing cartridge (DMC-11610) conjugated with the printer are used in this research in fig. 7 (b). The ink cartridge of this printer has a nominal volume of 10pL ink droplet when drops are dispensed from the cartridge head to the surface [41]. Since the printing is usually performed at room temperature (25°C), this inkjet printer is convenient to print on a variety of substrates, including low temperature plastics. Additionally, during deposition, surface topology is also not an issue due to its contactless printing technique. This printing technique can also fill the contact of multi-layer interconnection without any obstacle. It is also possible to print multiple layers of different materials on top of each other's.

The cartridge head consists of 16 nozzles with diameter of 21μm each. These nozzles can jet out ink simultaneously [41]. The process of jetting out ink is based on piezo

MEMS technology. Printer head has circular calipers/scale by which it is possible to tilt the angle of the printing head with respect to the plane of the platen as well as substrate. By doing this the resolution of the images can be controlled.

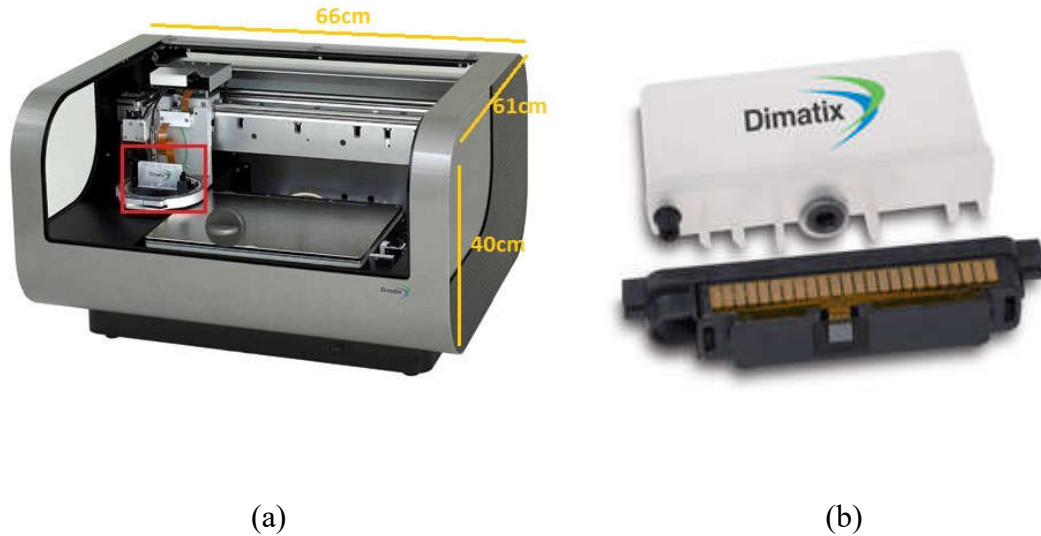


Figure 7. Fujifilm Dimatix material printer system. (a) Fujifilm Dimatix material printer and (b) reservoir and cartridge head [12]

Effect of Cartridge Angle on the Printing Resolution

Fig. 8 (a) shows the schematic of print head along with a mounted fiducial camera in the very left, cartridge cable, cartridge holder, holder latch and skew plate etc. Fiducial camera is operated by a control software Dimatix drop manager. It is used to set print origin, reference point, offsets calculation and real time line length width measurement value. Fig. 8 (b) is the enhanced schematic of circular calipers which are used for the setting angle between print head and cartridge head. This circular scale must be reset every time there is a change in the set value of drop spacing. Drop spacing is the center to center distance between two drops along the y-axis. Nozzle to nozzle distance in the x-axis is $254 \mu\text{m}$. So, if no modification is done, then the angle between platen and print head is maximum which is a 90° . Distance of deposited one drop to another in x-axis and y-axis is also $254 \mu\text{m}$ [41].

By setting the drop spacing value, angle between print head and platen is manipulated. Lower drop spacing results in higher density of ink in the deposited area thus the image resolution is high.

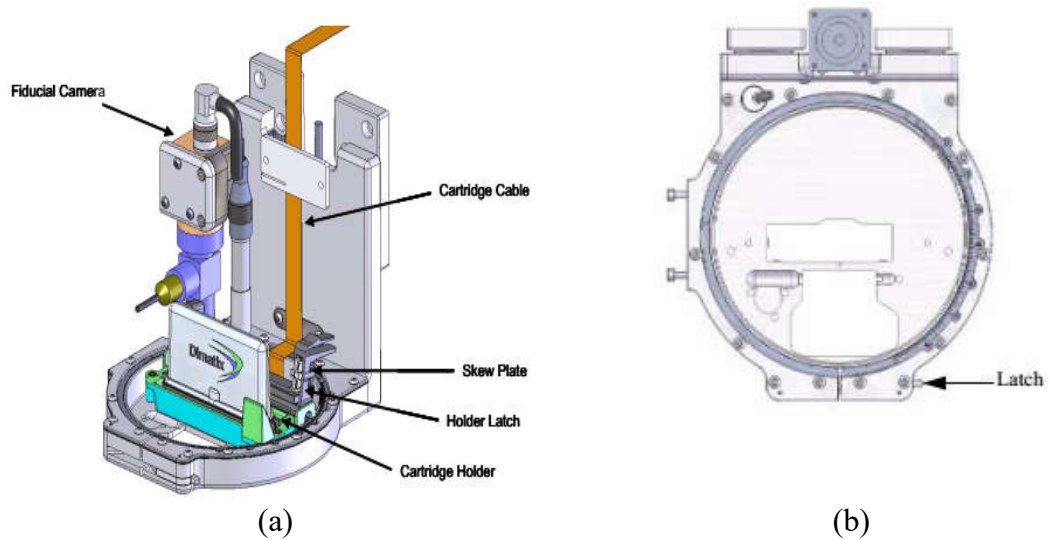
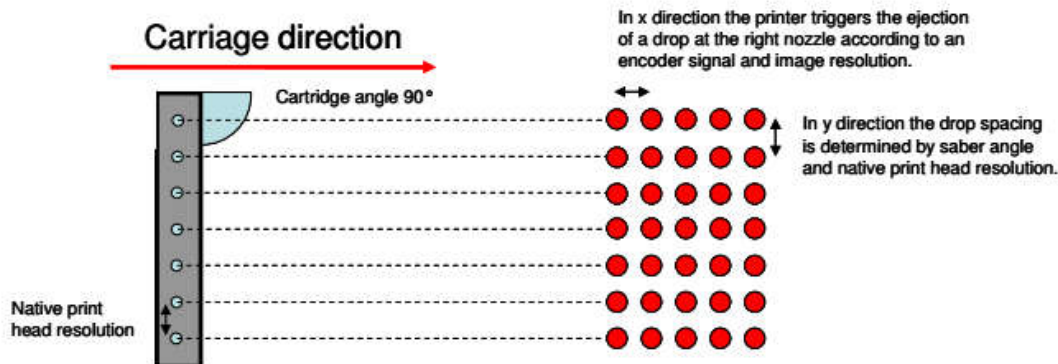
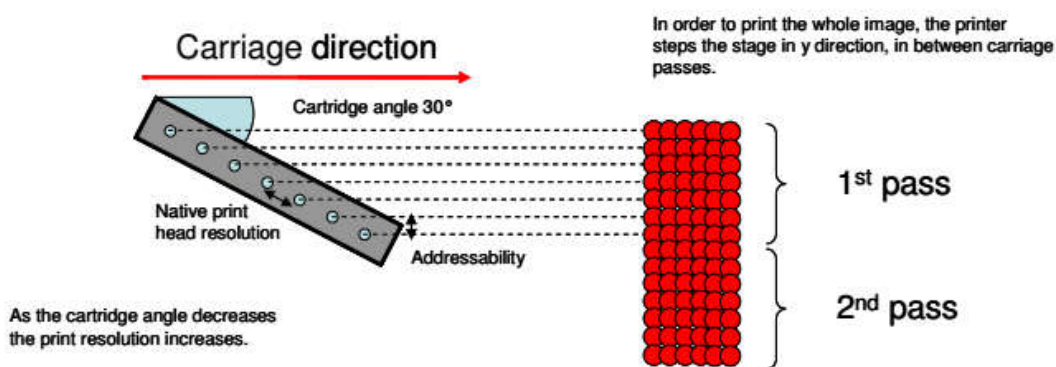


Figure 8. Print carriage or printer head system. (a) Print carriage and (b) carriage latch [42]

The effect of cartridge angle on the printing resolution is shown in fig. 9. It shows the smaller cartridge angle will provide high printing resolution with good area coverage due to the higher density of ink deposition on printed region. Ink density and the material deposition is higher. The cartridge angle is calculated by an internal image conversion software ACE 300 by putting a drop spacing value. Same drop spacing may not result the good printing for different types of ink.



(a) Larger cartridge angle. Angle between cartridge head and substrate is 90°



(b) Smaller cartridge angle. Angle between cartridge head and substrate is 30°

Figure 9. Relationship of cartridge angle versus material deposition. Smaller cartridge angle can provide higher printing resolution with good coverage area [43]

Droplet Formation by MEMS Technology

Piezo MEMS technology is used to design the print head. Operating procedure for the piezo MEMS inkjet technology shows in fig. 10. At first, a voltage waveform is developed for each type of material to be deposited. This predetermined voltage waveform is then applied in three different phases of operation to each of the 16 piezo MEMS valves. This controlled voltage in each nozzle will later form droplets.

Total droplet formation process follows the following steps:

1. Previously developed voltage waveform is applied in PZT bimorph (fig. 10 (b)). The fluid chamber is decompressed by the bias voltage. Fig. 10 (a) shows the starting and standby position of the pumping chamber.
2. In phase I, the voltage is decreased to zero volts at the beginning of each jetting cycle. After that, at maximum voltage it brings the piezo MEMS back to a neutral, straight and relaxed position. (Fig. 10 (b)).
3. The next two phases, phase 3 and phase 4 are the drop ejection cycle. The fluid chamber or reservoir compressed to generate enough pressure to eject droplets (fig. 10 (c)). The PZT motion is also controlled to form a droplet, but in this phase, due to the surface tension of the material, fluid does not detach from the cartridge.
4. In phase 4, the piezo voltage is brought back to its bias level. Thus, this phase of operation is called the recovery phase. The chamber decompresses again, which causes the separation of droplets from the nozzle. And finally, deposited on the substrate (fig. 10 (d)) [41].

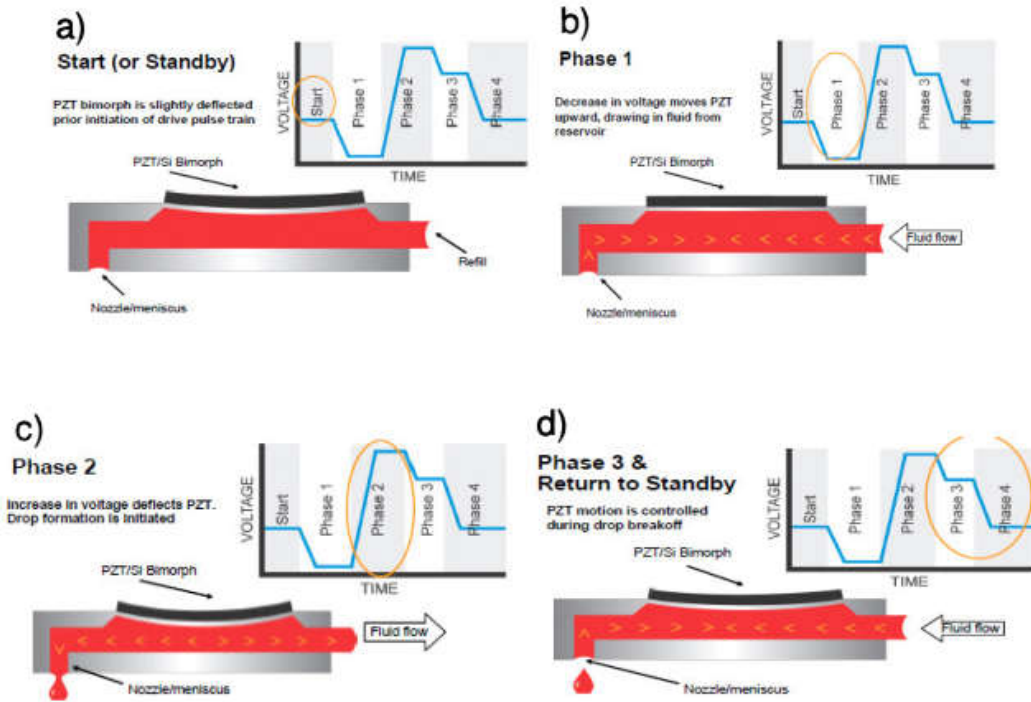


Figure 10. Formation of a droplet in the nozzle [41]

Understanding the cartridge head operation will help to design the waveform for each type of material ink. Notice that the drop was formed in phase 3 (fig. 10 (c)) at the tip of the nozzle but jetted out only at the end of phase 4.

Device Fabrication by Inkjet Printing

Flexible Electronics Fabrication by Printing Process

The purpose of this section is to serve a guide for flexible electronics fabrication by inkjet printing technique. Printing is what we do in everyday life so it seems to be an easy task; however, to print in large scale as a form of circuit device or in very small scale in micro-nano range, it is not as easy as thought. To prevent the deviation in operation of these nozzles, testing of each of the 16 nozzles is necessary before any printing operation. It is found from literature review and other experimental work, for small pattern or feature printing, usage of one nozzle provides more consistent results, than using multiple nozzles.

The orientation of the device or designed circuit needs to be considered for large area printing, with small and large structures or even lines next to each other. Fulfillment of this criterion is necessary so that the printing material can be deposited uniformly. It is found that small lines located next to each other and large area printing together produces a poor device. This is because of the continuous operation of the nozzles. During long operation time or jetting time, the printing material wets the nozzle surface. Thus, jetting misfires by the previously stored wet liquid ink on nozzle surface. Additionally, the performance of the nozzle degrades after printing a large area where the nozzles provide uniform deposition at the beginning of printing.

Resolution Limit

The achievable minimum line width and spacing dimensions specified by manufacturer are $100\mu\text{m}$ for their specified ink [41]. However, different types and manufacturer's ink can perform differently. For example, a wet type or water based ink can spread quickly on the substrate; the line can be wider or bigger than specified. Another property may be responsible for resolution limit control is adhesion property between substrate and ink. This property can be controlled by surface cleaning and oxygen plasma treatment of the surface of the substrate.

Two types of conductive ink are used throughout the research. PEDOT (Poly(3,4-ethylenedioxythiophene)-poly(styrene sulfonate)) high-conductivity grade from Sigma Aldrich, used for transmission line and cantilever fabrication. Metalon silver ink (JSB-40G) from Novacentrix, used for sacrificial layer. Viscosity of the silver ink is about (8-10) cP with surface tension (28-32) dyne/cm [44]. On the other hand, PEDOT is a water based ink with high viscosity and surface tension. Deposition of PEDOT on top of kapton

is difficult as it is a water based ink and surface of the substrate is hydrophobic. So, the surface of the substrate needs special treatment and special printing environment for good printing with PEDOT ink.

It is also observed that, by setting minimum distance between cartridge nozzles and substrate, and lower waveform triggering voltage of around (20-26) V, it is possible to achieve smallest printed structure sizes during ink deposition. Also, using only one or two nozzles at a time during printing results in good outputs.

Material Evaluation

Below are the evaluation results for the electrodes, cantilever beam and sacrificial layer for the MEMS switch.

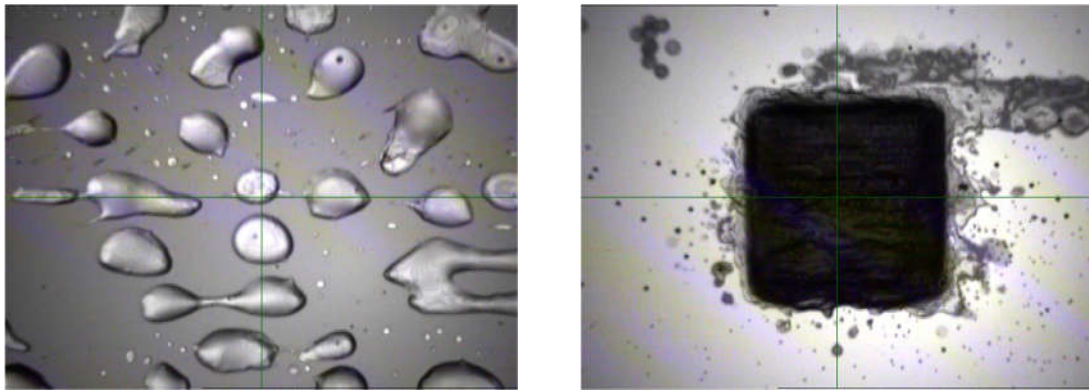
PEDOT Ink Evaluation

PEDOT is used to fabricate two of the most important portions of the printed MEMS switch namely transmission lines and cantilever. The reason behind choosing PEDOT for these two parts is its remarkable properties. The most important property of PEDOT is the reasonable viscosity which makes it possible for using it for inkjet printer. Also, it is a polymer type ink and not reacted with acid which is a very specification and requirement for our application. Table 5 shows the typical properties of PEDOT [45]:

Table 5. Typical properties of PEDOT [45]

Visual appearance	Dark blue liquid
Solid Content	0,8 wt%
Viscosity	7 – 12 cP
Surface Tension	31 – 34 mN/m
pH	1.5 – 3.0
Surface resistance	110 Ohm/sq
Shelf life	6 months

PEDOT is stored between 4°C – 25°C in a vacuum oven. As earlier mentioned, to achieve a good printing by PEDOT, surface treatment of the substrate is needed. Fig. 11 shows the printing of PEDOT without and with surface treatment. Same pattern was set to print by PEDOT.



(a)

(b)

Figure 11. Surface treatment effect on PEDOT printing

It is seen that, PEDOT doesn't cover whole area when the surface is hydrophobic or untreated, it is just few drops although the designed file instruction is to have whole area coverage. On the other hand, there is a good coverage of PEDOT when the surface is made hydrophilic by oxygen plasma treatment with 100 watts for 5 minutes. So, it can be said that, oxygen plasma treatment increase the adhesion property of surface for PEDOT.

Oxygen Plasma Treatment (Surface Treatment)

Oxygen plasma treatment of the surface of kapton substrate is done to achieve two main aspects; one is to clean the surface and second is to increase the adhesion property. The Oxygen plasma process has done in a low pressure and oxygen gas discharge chamber. After the material or specimen is loaded, the chamber is evacuated to a vacuum pressure of (0.1-0.2) torr using a mechanical pump. Fig. 12 shows the RIE system (NRE-4000) used

in this research for oxygen plasma treatment. The NRE-4000 is a Reactive Ion Etching (RIE) system with a shower head gas distribution and a water-cooled RF platen. It can accept up to 8 inch wafers. The power for the system is provided by 600W 13.5MHz power supply, and 1000W auto-tuner. The DC bias reaches as high as -500V, it is important for anisotropic etching.

Oxygen plasma treatment grows a thin layer of di-oxide on top of the surface. The oxygen molecule from oxide layer that can bond with the water portion of the water based ink such as PEDOT. By this way, this process increases the chemical bonding between the ink and surface of the substrate thus adhesion property also increased.



Figure 12. Typical RIE chamber for oxygen plasma treatment while plasma treatment [46]

Printing Parameter Setting for PEDOT Ink

It is recommended by the manufacturer to filter the PEDOT every time before printing. Typical filters that can be used are hydrophilic type filter such as a syringe filter of 0.2 μ m or 0.45 μ m [45].

It is recommended to give a gentle shake to the PEDOT before load the ink in the reservoir. This gentle shake will homogenize the PEDOT ink solution. Cleaning the cartridge head and nozzles are also another important step to achieve a good print with this polymer ink. Finally, fill out DMC-11610 cartridge by the ink with the help of plastic syringe and a 0.45 μ m filter connected to the needle. While attaching the reservoir with cartridge head it is necessary to make sure there is no air present in the cartridge. Sometimes 30-90 minutes of waiting time is needed to dissolve all the tiny air bubbles in the print head to achieve proper operation [45]. After a continuous printing, the nozzle plate needs to be wiped with a lint free clean-room cloth.

In this research for PEDOT printing, the firing voltage setting for print head is used as: (20-25)V, firing frequency: 5KHz and cartridge temperature: 24°C. The platen temperature was held at 38°C during printing [45].

Silver Ink Evaluation

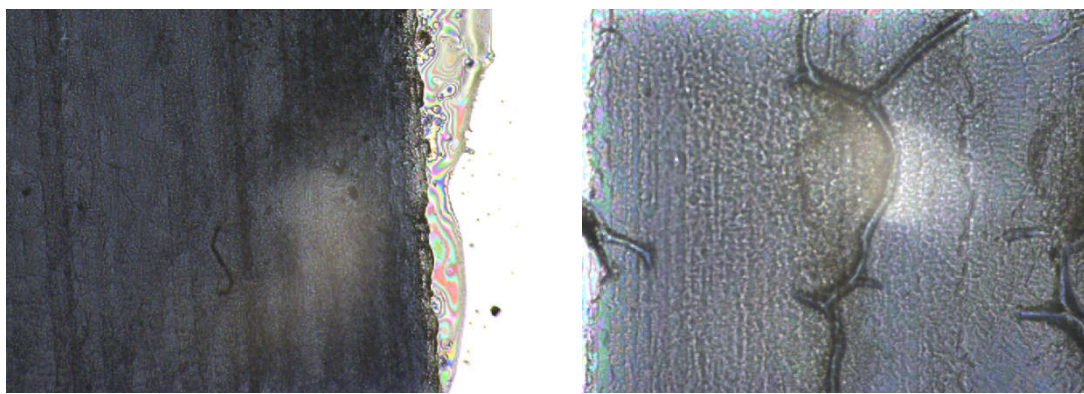
In the prototype, MEMS device fabrication, silver is used as a sacrificial layer. That means, after the complete device fabrication silver is etched away to create the dielectric air medium in between the transmission lines and cantilever. Metalon silver ink is highly conductive at standard curing temperature (120°C for 10min and 220°C for 30min). After a standard curing process, a 1cm by 1cm silver patch gives 1.22 Ω resistance with a thickness of 0.75 μ m. In this research, it is not necessary for the silver ink to be conductive,

rather it needs to be etched away quickly without disrupting other layers. But it is found that, standard curing temperature needs higher time to completely etched off the silver layer. Table 6 shows the etching rate of silver for standard temperature curing condition. At total of 4 samples were prepared for this test with different curing temperature and printing conditions.

Table 6. Evaluation for silver ink

Print	Total layers	Curing Condition	Thickness (μm)	Etching Time	Etching rate ($\mu\text{m}/\text{sec}$)
Sample 1	4 layer together	100C@10min 200C@20min	1.92	28min 23sec	0.0011
Sample 2	1+1+1+1	100C@10min 200C@20min	1.98	17min 39sec	0.0019
Sample 3	4 layer together	65C@20min 100C@20min	2.795	11min 50sec	0.0039
Sample 4	1+1+1+1	65C@20min 100C@20min	2.005	1min 40sec	0.02

Additionally, high temperature curing also damaged the PEDOT transmission line which is deposited just before sacrificial layer. Fig. 13 shows that PEDOT transmission line cracked after high temperature curing of silver.



(a) 65° C curing

(b) 200°C curing

Figure 13. High temperature curing effect on PEDOT printing

Although low temperature curing significantly increases the etching rate without damaging the PEDOT layer, but there are still problems due to the low temperature cured wet silver. Because of this, deposition of the next PEDOT layer (cantilever) on top of wet silver becomes difficult and even for sometimes impossible. Finally, a critical curing temperature of 150°C for 15 minutes was found which solves almost all the problems. After that, this curing temperature of silver is used throughout the research. Also, it is found that, the etching solution with a higher acid ratio also improves etching rate of Metalon silver ink.

Etching Solution: The Ag etching solution is HAC (CH₃COOH): H₂O₂: H₂O in proportions 1:1:10 or 2:2:10 or 2.5:2.5:10 (where HAC stands for acetic acid). H₂O₂ is Hydrogen-per-oxide solution 30% (weight/weight) in H₂O.

Kapton Substrate Evaluation

Kapton film (HN type) of thickness 5mil or 125µm from Dupont is used as substrate in this research. As per manufacturer specifications, kapton film can be used at temperatures as low as -269°C and as high as 400°C [47]. Kapton film is chosen as the substrate for this work due to its flexibility, high temperature operability (400°C) and low elastic coefficient.

As acid etching is one of the important step during device fabrication, it is also important to choose a substrate whose performance doesn't degraded by acid. Kapton's performance does not affected due to acid treatment; this is one of the important reason to choose kapton as substrate.

MEMS Switch Fabrication

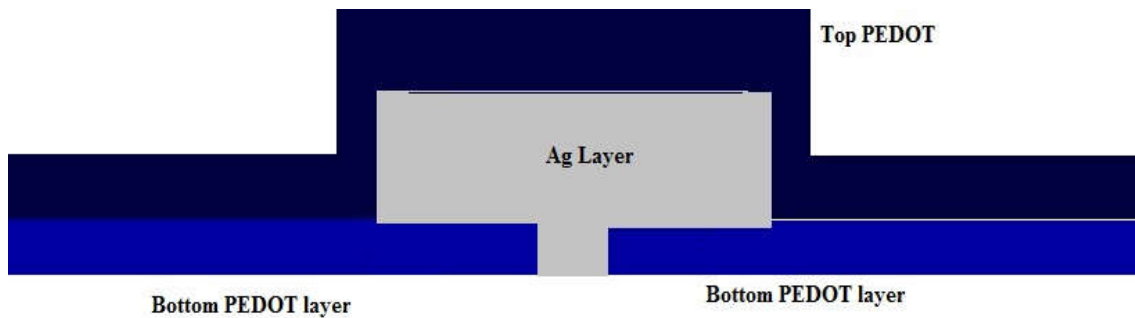
Schematic of Fabrication Steps of Typical MEMS Switch

To simplify the later discussion, a typical switch fabrication flow is provided in fig. 14. In this figure, the bottom and top electrodes are deposited using poly(3,4-ethylenedioxythiophene) polystyrene sulfonate (PEDOT) on top of kapton polyamide. Then the sacrificial layer (Ag) is deposited and patterned in between the top and bottom electrode. After completion of the whole fabrication process, the total sacrificial layer area is etched to create a dielectric medium of air. This is achieved by etch time control with an appropriate etching solution. Finally, the top electrode serves as the cantilever beam and the bottom electrodes as transmission lines. Finally, the total fabricated switch is released by removing the sacrificial layer.

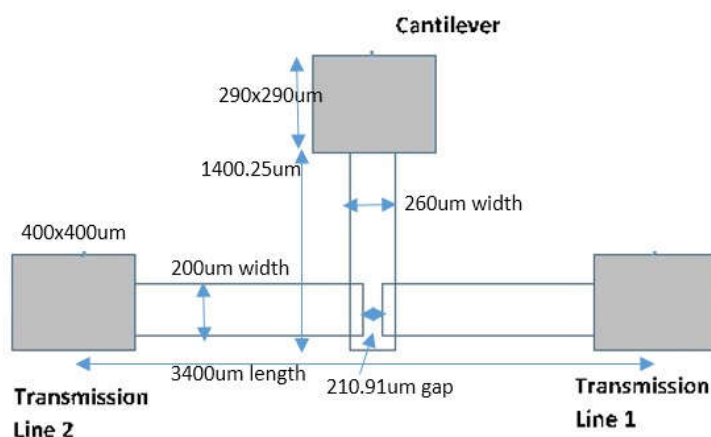


Figure 14. Switch process flow. (a) deposition and patterning of bottom electrode. (b) deposition and patterning of sacrificial layer. (c) deposition of top electrode as cantilever beam(d) plating cantilever beam, removing sacrificial layer to release the beam [48]

Fabricated MEMS switch is a three-layer device; bottom PEDOT layers (as two separate transmission lines), Ag sacrificial layer and top PEDOT layer (as cantilever). Fig. 15 (a) shows the schematic front view of the designed MEMS switch. Top view with critical length and width of fabricated device is shown in fig. 15 (b). From the figure, it is seen that two-transmission line has a separation of $210.91\mu\text{m}$ and the length and width of cantilever is respectively $1400.25\mu\text{m}$ and $260\mu\text{m}$. Three contact points are also printed in three terminals of the switch. Two end of the transmission lines contact has a dimension of $400\mu\text{m}$ by $400\mu\text{m}$ and the cantilever end contact has a dimension of $290\mu\text{m}$ by $290\mu\text{m}$. It is to be mention that; the cantilever contact point dimension is less than other two to achieve a minimum weight of cantilever portion.



(a)



(b)

Figure 15. Schematic of fabricated MEMS switch. (a) front view of designed MEMS switch (b) top view with critical length and width of fabricated device

The weight of the cantilever and whole device is important as this switch has two operational parts; electrical part and mechanical part. When the weight of the cantilever is high then following, problems happened during the test device fabrication, (i) just after removal of sacrificial layer, the cantilever automatically pulled-down without even applying test voltage. (ii) other problem was, even if the cantilever still stay hanging and didn't pull-down automatically, then switch needed very high turn-on voltage (more than 60V) to completely pull-off the cantilever to bottom electrode. To overcome these two-inherent problems, a critical thickness of PEDOT cantilever and all layers were calculated. Table 7 shows the critical thickness of top PEDOT, middle sacrificial and bottom PEDOT layer, which maintained during final device fabrication.

Table 7. Designed critical thickness of each layer

Steps	Sequence of Print	Materials	Thickness	Curing Conditions
1	Transmission lines	PEDOT	1 μ m	100°C for 10 minutes
2	Sacrificial layers	Ag	3 μ m	150°C for 15 minutes
3	Cantilever	PEDOT	2 μ m	100°C for 10 minutes

Creating Design File

Layer by layer design file is created using AutoCad 2017 educational version. Fig. 16 shows the schematic of AutoCad design file. After design, this file is saved as either .dxf file or gerber file. Then, with the help of other two software ACE 3000 and Dimatix drop manager, the file is converted to a printable format.

Dimatix drop manager motion control software has some other important features rather than only converting bmp file to .ptf file format. Two most important features are fiducial camera and drop watcher. Fiducial camera enables the viewing of real time printing, set print origin and reference point etc. And drop watcher facilitate the observation of the drop by drop video of 16 nozzles [41]. Voltage setting, cartridge temperature setting, nozzle selection before printing can be done using drop watcher.

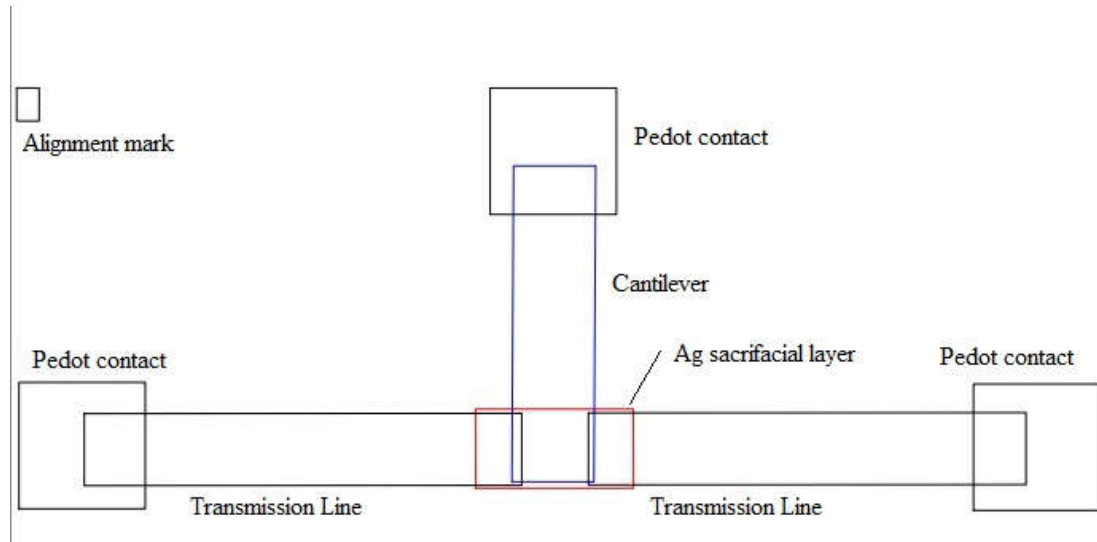
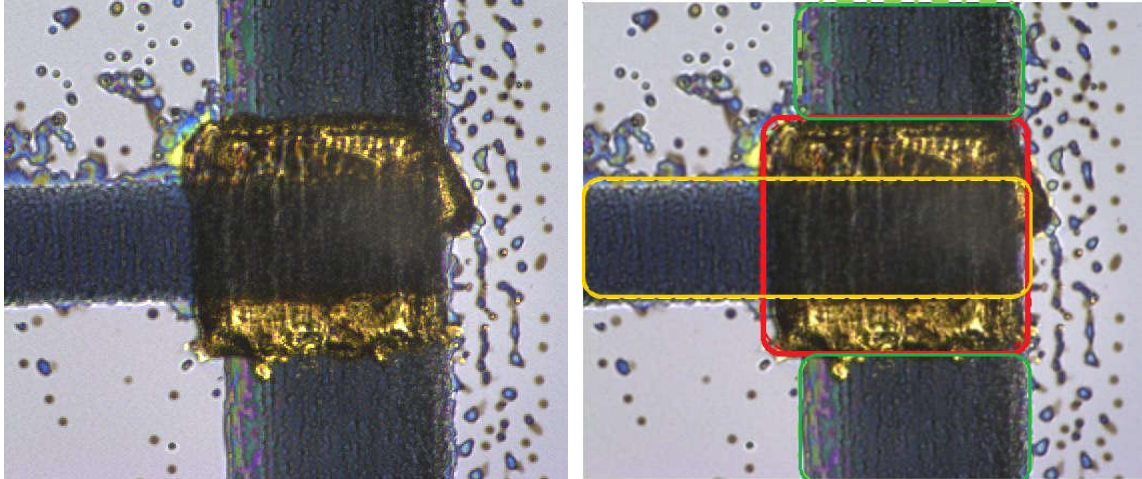


Figure 16. Layer by layer design file created by AutoCAD 2017

Using the software, ACE 3000, previously saved .dxf or gerber file are converted to .bmp or matrix bitmap image format. ACE 3000 is a conjugated image conversion software that comes with the Fujifilm Dimatix material printer. All the printing parameters are set using this software such as drop spacing, cartridge head angle, printing scaling unit and pattern size during printing etc. Also, using this software, it is also possible to modify further before printing. Finally, another software Dimatix drop manager convert the pattern to a final. ptf format. Only. ptf formatted pattern can print the machine.

First Complete Printed MEMS Switch

Fig. 17 (a) shows top view of the fully printed MEMS switch. Three different layers is marked in fig. 17 (b). Green pointed region is the bottom PEDOT as transmission lines, Red pointed region Ag sacrificial layer and top PEDOT as cantilever.



(a)

(b)

Figure 17. All three layers of device and cantilever. Green: representing bottom PEDOT layer. Red: representing Ag layer on top of PEDOT. Yellow: representing top PEDOT layer of device.

Table 8 shows the thickness and width of each layers after printing. It is seen that, the designed thickness for bottom PEDOT, sacrificial layer and top PEDOT was respectively $1\mu\text{m}$, $3\mu\text{m}$ and $2\mu\text{m}$, but after printing following thickness is found. Although this thickness could be still well controlled by controlling number of layers.

Table 8. Final thickness and width of each layers of printed switch

Layer name	Materials	Thickness after print	Width
Bottom layer	PEDOT	$1.74\ \mu\text{m}$	$265\ \mu\text{m}$
Sacrificial layer	Ag	$4.13\ \mu\text{m}$	$380\ \mu\text{m}$
Top layer	PEDOT	$2.76\ \mu\text{m}$	$345\ \mu\text{m}$

It is observed that after printing each types of ink have some deviation from its print origin. This deviation in called offset. After first layer of printing it was necessary to record the offset value to get rid of alignment issue during next time. Offset could occur in both x-axis and y-axis or any of single axis.

Offset for PEDOT ink was found to be +104 μ m in x-axis and -349 μ m in y-axis. The offset value for Ag ink was -102 μ m in x-axis and -181 μ m in y-axis. Table 9 shows the printing parameters during the print of each types of material ink.

Table 9. Set parameters during the printing of each type of material ink printing

Material Ink	Nozzle Voltage (V)	Drop Spacing	Angle between Print head and Cartridge (degree)	Meniscus point	Platen Temperature ($^{\circ}$ C)	Cartridge Temperature ($^{\circ}$ C)
PEDOT	30	25	5.6	4.0	38	26
Ag	26	35	8.2	4.5	48	28

In this chapter, the step-by-step fabrication process and inherent problems during fabrication is discussed. The chapter started with Fujifilm Dimatix material printer deposition technique, then material evaluation process and ends with the fabrication of first successful printed MEMS switch.

V. DEVICE TESTING AND DC ANALYSIS

Introduction

This chapter contains full fabrication process and the experimental results of an inkjet printed MEMS switch. The prototype switches have gone through stepwise evolution process and after each evaluation, the result shows the direction for the modification needed before next batch fabrication. In this discussion, each of the individual test device will be described and an effort will be made to specify the type of switch being investigated. It is worth mentioning that after every batch there were some design modifications which tends toward fabricating a consistent package of device. Also, similar tests are performed on many devices to see the consistency of device performance.

The following sections includes instrumentation used for this research, MEMS switch characterization and DC analysis of the switch.

Instrumentation (Software and Hardware)

This section discusses the pre-and *post*-fabrication conditions for the MEMS switch testing purpose. Later, a brief description is given for the hardware and software employed to perform the tests. As mentioned in chapter 4, Fujifilm Dimatix material printer is used to fabricate complete batch of devices. In the pre- and post-fabrication stage, some other instruments are also used, namely KLA-Tencor, four-point probe resistance measurement system, multimeter and external power supply etc. Fujifilm Dimatix material printer and KLA-Tencor surface profiler comes with integrated control software to ease the experimental set up and automation of the testing.

The following sections briefly discuss the purpose of the individual hardware and software tools used in this research.

KLA-Tencor

The KLA-Tencor profiler usually used for the determination of thin film step height measurements, thick film step height measurements, etched trench depth, materials characterization for surface roughness and waviness, surface curvature and form, 2D stress of thin films, dimensional analysis and surface texture, 3D imaging of various surfaces, flatness or curvature, defect review and defect analysis and many more. The surface measurement system has maximum 150mm scan length in x-axis. The sensor of the KLA-Tencor includes dynamic force control, excellent linearity, and the highest vertical resolution. The ultralight and ultra-sensitive sensor prevent the sample to be destroyed any-time during scanning operation. The profiler used in our research is a P-7 stylus KLA-Tencor profiler.

Apex Software

It is an advanced filtering software contains leveling, and analysis functions to support production environments. This also includes over 40 key parameters such as surface depth, step height, roughness, waviness, slope, flatness, radius of curvature, stress etc. Apex also has a simple and intuitive format that allows the users for an easy creation of pdf reports and automatic data processing. In this research, after taking 2D and 3D scan by the P-7 stylus profiler, collected raw data was analyzed by *APEX* software to reach conclusive results.

4-Point Probe Resistance Measurement

The four-point-probe resistance measurement technique is a well-accepted method for resistance or resistivity measurement. It does not have the parasitic resistance in the leads. That's why the data measured are more accurate than other methods. In this research, a Keithley 2800 4-point probe system is used to measure sheet resistance. This instrument is used in the pre-fabrication stage during material evaluation.

Device Characterization

Test Device: 1

Fig. 18 shows the first fabricated inkjet printed MEMS switch. Although this device plays an important role in proposing the appropriate approach of making a successful device. This design consists of two metal contacts as transmission lines, an anchor, and the top electrode makes a cantilever beam portion, and finally, a dielectric layer is positioned between the cantilever beam and the transmission lines. Fig. 18 (a) is the top view of the design and Fig. 18 (b) is the side view.

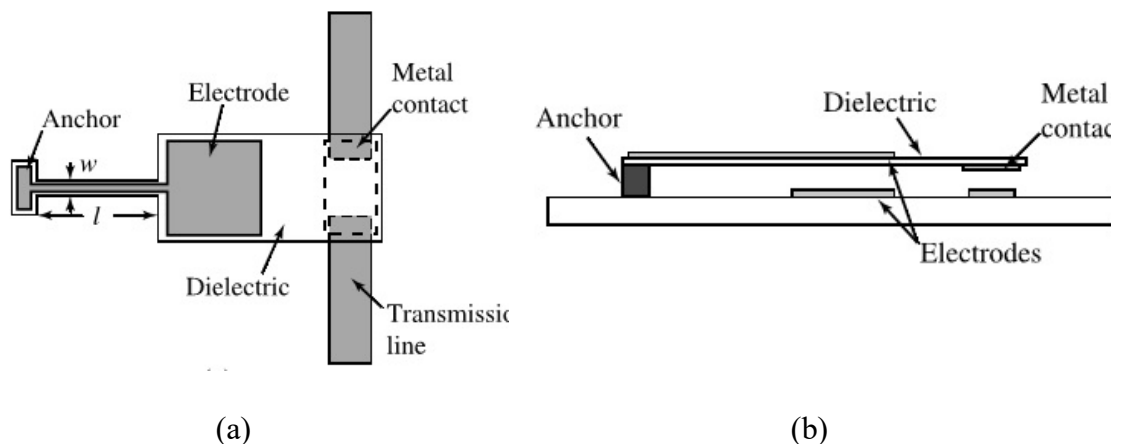


Figure 18. Top and side view of modeled MEMS switch. (a) top view (b) side view [49].

The basic working principle of this device is similar to dielectric breakdown process due to a certain voltage applied [49]. In normal condition the path via dielectric layer from the anchor or cantilever beam to transmission line remains open. The breakdown between the cantilever beam and transmission lines may occur at certain voltage. As a result, the path from the cantilever beam to transmission lines via dielectric layer will shorten and the device will be turned on.

Material Selection and Evaluation

Table 10 shows the material selection for the first fabricated fully printed MEMS switch. In the very first fabricated switch, silicon was used as base substrate and the base layer material was Ag nano-particle ink from Novacentrix. As silver is a high conductive material ink, so it was used to fabricate transmission lines. Polymer conductive ink PEDOT was used to print cantilever beam. It is to be noted that, due to its polymer and light weight property, after membrane release it was assumed not to fall-down the cantilever beam on transmission line automatically. But PEDOT cantilever may start damping due to the shaking of the device during etching and moving from one beaker to another. Curing condition and temperature environment setting are taken from manufacturer but some of the curing conditions were still needed to modify for our application purpose.

Table 10. Material evaluation for very first fabricated device on silicon substrate

Steps	Layer name	Material Selection	Designed Thickness	Curing condition
1	Transmission lines	Ag	1 μ m	100°C @ 10min and 200°C @ 30min
1.5	Protective layer	PEDOT	2 μ m	100°C @ 10min
2	Sacrificial layer	Cu	2.5 μ m 4 μ m	50°C @ 1hr Or

				220°C @ 1hr in 300 SCCM (Ar) + 30 SCCM (H ₂)
3	Cantilever	PEDOT	4μm	100°C @ 10min

First Fully Printed MEMS Switch

Fig. 19 shows the schematic of first designed MEMS switch which had four-layers in total. After each layer printing sample taken off from the printer platen for curing. After curing every printed layer, it was a challenge to finding the exact print origin used to print previous layer. To get rid of this problem, a square on the top left corner of the diagram is used as an alignment mark which is not a part of the main device.

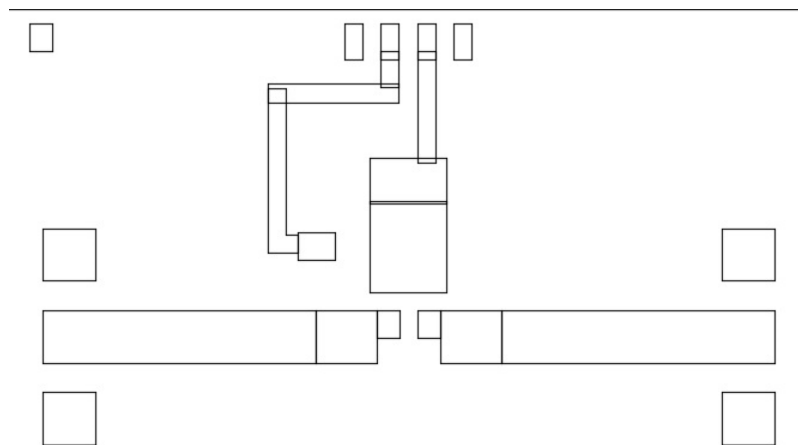


Figure 19. Schematic of printed MEMS switch

First Tested MEMS Switch

Fig. 20 (a) shows the first printed base layer by Ag nano-particle ink. The silver nano-particle ink deposited uniformly with a thickness of 0.75μm for first printed layer. Fig. 20 (b) shows the first Ag printed layer with PEDOT protective layer on top of Ag transmission lines. PEDOT is used as protective layer because it has a chemical property not to react with acid solution. PEDOT has a thickness of 0.04μm ~ 0.06μm for one printed layer. Here total 12 printed layer is taken due to fulfillment of the critical thickness requirement.

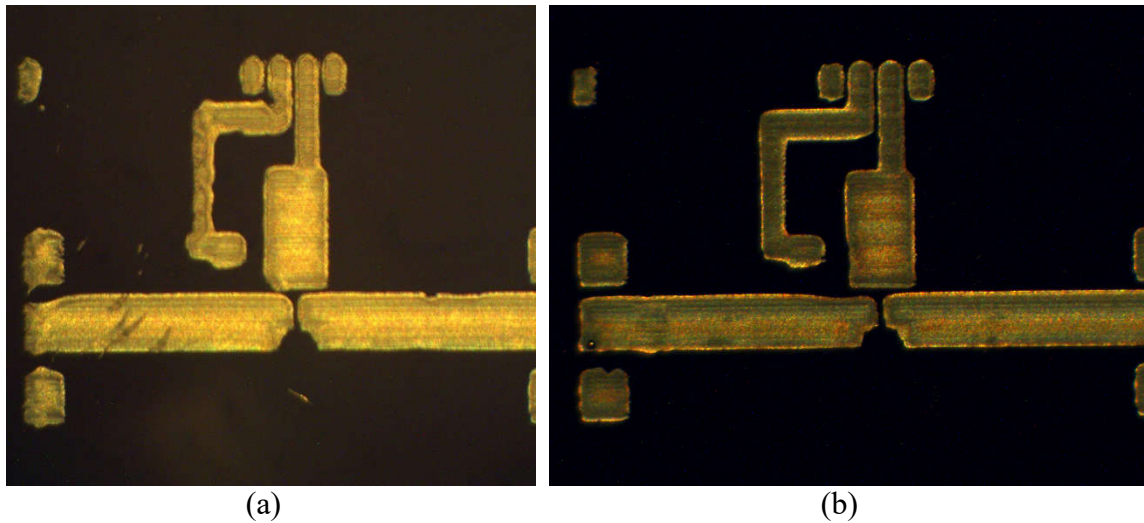


Figure 20. (a) First printed layer by Ag ink (b) first and second layer (Ag and PEDOT)

Sacrificial Layer Deposition and Etching

Inkjet printable Cu ink is used for the sacrificial layer deposition in between top electrode and bottom electrode. It is found that a single layer of printed Cu has a thickness is about $0.7\mu\text{m}$. Fig. 21 shows the thickness measurement by KLA-Tencor for first printed Cu layer. After choosing an appropriate scan recipe for metallic Cu ink, a 2D scan has taken. Raw data is then analyzed by *APEX* image processing software and thickness is shown as step height. Step height or thickness measurement is necessary at this stage to calculate the etching rate.

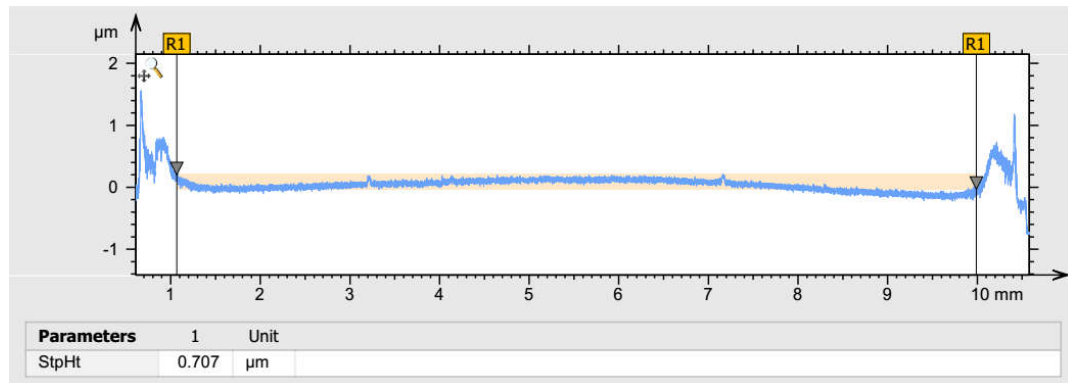


Figure 21. 2D analysis of the Cu sacrificial layer

After taking the thickness measurement of the sacrificial layer, following steps has followed to accomplish the etching process of single layer printed Cu.

1. The Cu etching solution is an acid solution of HAC (Acetic Acid): H₂O₂: H₂O in proportions 1:1:10 or 2:2:10 or 2.5:2.5:10 (where HAC stands for acetic acid). H₂O₂ is Hydrogen-per-Oxide solution 30% (weight/weight) in H₂O.
2. Cu sacrificial layer completely etched of within around 82 seconds. So, the etching rate was calculated as 0.008 μ m/sec.

Fig. 22 shows the fully printed four-layer device when Cu is used as sacrificial layer. This image is taken by AmScope before the Cu etching process.

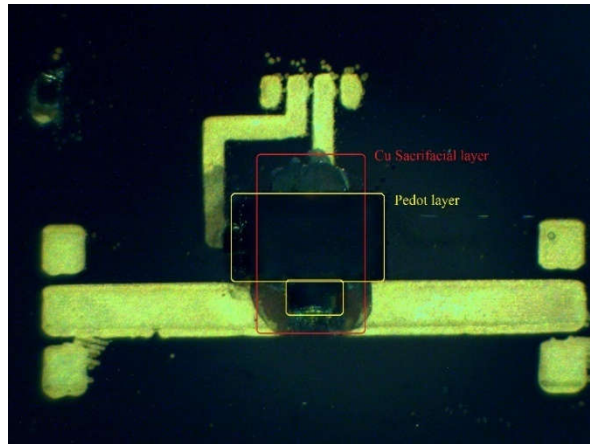


Figure 22. Complete device on silicon substrate with Cu sacrificial layer

The yellow pointed boxes are top electrode or cantilever beam, printed by PEDOT with thickness of about 4 μ m and the Cu sacrificial layer has a total thickness of about 2.1 μ m.

Releasing Membrane

Previously used etching solution is used to release membrane by removing Cu sacrificial layer. After every 5-10 minutes, etching condition is recorded to check if the sacrificial layer completely went off or not. It is a very important step not let to dry out the device

during etching and checking. Three beaker steps are followed: acid to acetone, to IPA, then to microscope. Every time slowly and carefully the device is transferred from one beaker to another, by doing the three beaker steps, the liquids are not completely shaken off from the device. After observation under microscope, the sample is put back to the acid solution very quickly for further etching. This process is usually repeated till the Cu sacrificial layer is completely etched away.

The etching of complete Cu sacrificial layer took almost 42 minutes. There are total three-layer printed Cu with a thickness of about $2.1\mu\text{m}$. And etching rate is about $0.0008\mu\text{m}/\text{sec}$ which doesn't support the previously achieved experimental result, $0.008\mu\text{m}/\text{sec}$. This could be because of few reasons as- (i) the $4\mu\text{m}$ thick printed PEDOT cantilever on top Cu sacrificial layer was protecting Cu sacrificial layer. As PEDOT doesn't affected by the acid solution, it was working as a protective layer for the Cu sacrificial layer. (ii) Also, it was found that, Cu easily oxidize in open air and produce a copper oxide (CuO) layer on top Cu. So, it was also preventing the quick etching of Cu layer.

Fig. 23 (a) shows that, the Ag transmission lines are also etched away along with Cu sacrificial layer. Fig. 23 (b) Cu sacrificial layer is also not completely etched off after 15 minutes of etching time. The reasons of Ag etching are- (i) the weak bonding between Ag metallic ink and silicon substrate, (ii) $1\mu\text{m}$ thick PEDOT protective layer was not thick enough to protect the Ag layer and (iii) Ag is a metallic ink which easily react with the acid solution. First two problems were easily solvable by increasing the adhesion property between ink and substrate by oxygen plasma treatment and by increase the thickness of PEDOT protective layer by increasing number of printed layers. But the third problem was

not easily solvable which made us a replacement of Cu sacrificial layer by Ag ink and the Ag transmission lines by PEDOT for next device fabrication.

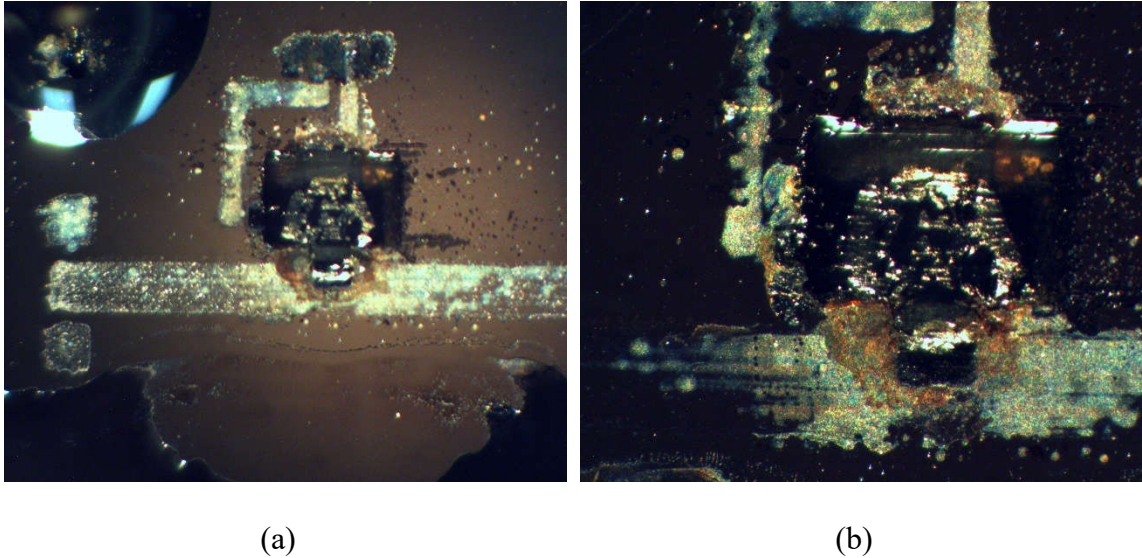


Figure 23. Cu etching test. (a) after 10 minutes (b) after 15 minutes

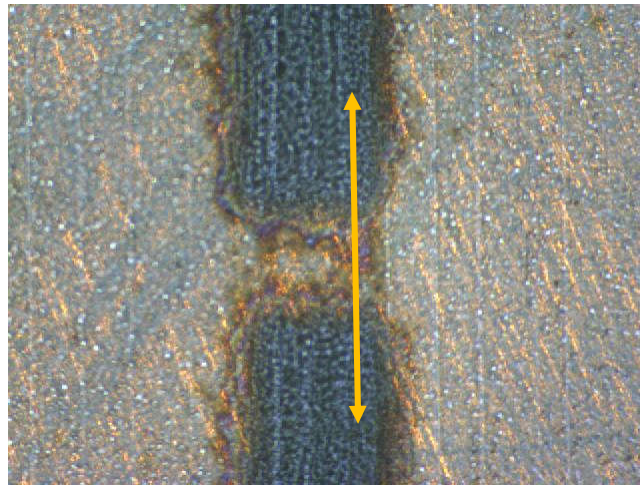
As the device destroyed in this stage of testing, further testing of this device was not possible. Next section discusses the first successful device fabrication and testing.

First Successful Device (Fabrication and Testing)

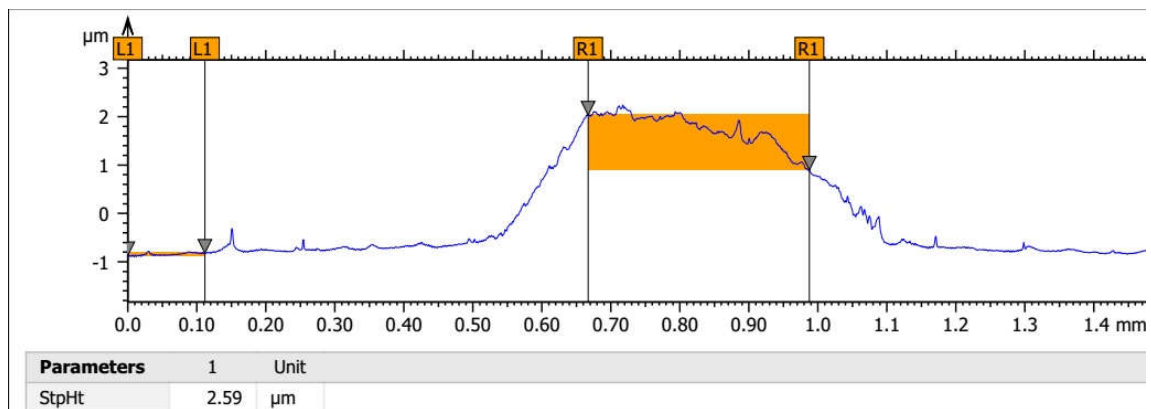
In this section, step by step evaluation of first successful device and dc analysis of the device is discussed. In chapter 4 the fabrication process and material selection is already discussed. Original design and materials for each layer of printing had to be modified before this batch of device fabrication. For this device, kapton is used as substrate material instead of silicon due to its application requirements. Also, the width of the cantilever was made smaller so that it doesn't have much weight to pull down automatically because of its own weight after removing sacrificial layer. This device is a three-layered device; bottom PEDOT as the transmission line, middle Ag as the sacrificial layer and top PEDOT as the cantilever beam.

Analysis of Bottom PEDOT Layer

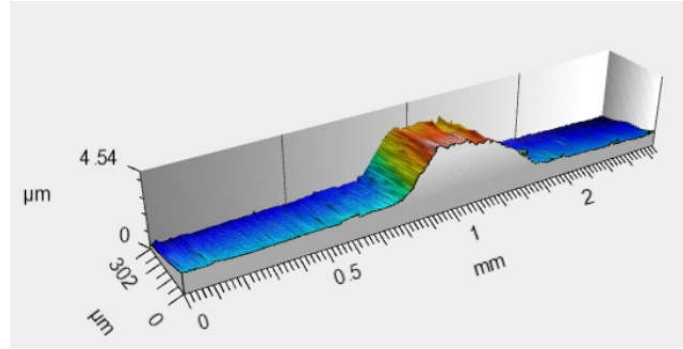
Fig. 24 (a) shows the image of first printed layer of the device which is the transmission lines deposited by PEDOT polymer ink, image is taken by KLA-Tencor process camera. This transmission lines have an average thickness of $2.59\mu\text{m}$. Fig. 24 (b) shows the 2D thickness measurement and fig. 24 (c) is the uniformity check by 3D analysis. This step needed total of 20 layers of printed PEDOT to achieve the designed critical thickness.



(a)



(b)



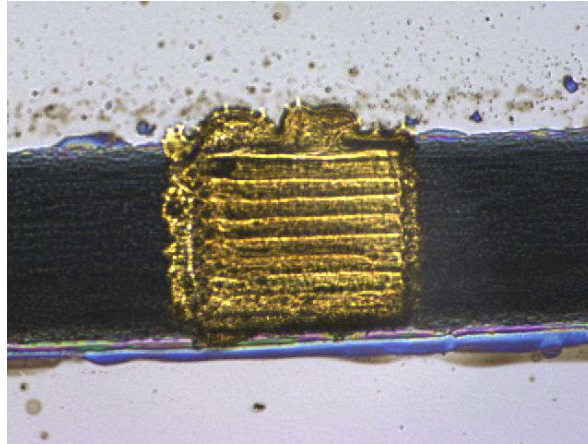
(c)

Figure 24. Printed PEDOT layer test. (a) First printed layer on kapton substrate (b) thickness measurement by KLA-Tencor (c) uniformity check by *APEX* 3D analysis

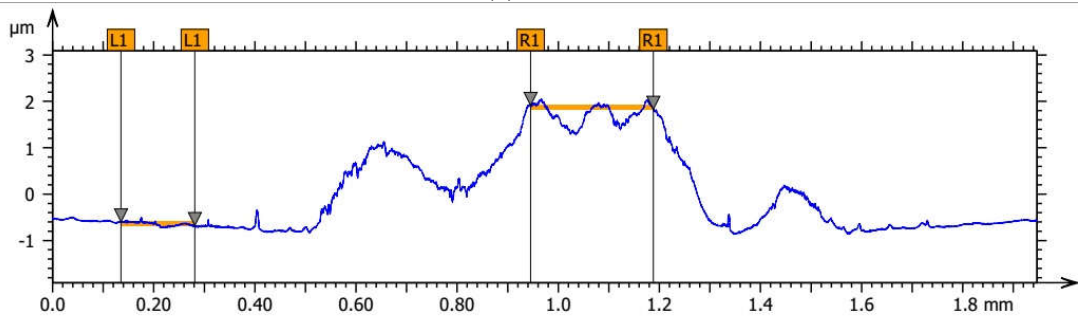
From fig. 24 (a), it seems that, the two-transmission lines are shorted a little bit. The reason behind this is the spreading of ink during printing. But the amount of PEDOT is quite small and the uniformity is not well enough to short the path. The measured resistance between two near points of transmission lines were found to be infinite which proved that the two-transmission lines were still disconnected. Additionally, self-resistance of a single PEDOT transmission line is measured as (1.1-2.0) K Ω .

Analysis of Ag Sacrificial Layer

Fig. 25 (a) shows the second printed layer which is Ag sacrificial layer of the device. Average thickness of this layer is about 2.35 μm . Fig. 25 (b) shows the 2D thickness measurement and fig. 25 (c) is the uniformity of deposited Ag metallic ink by *APEX* 3D analysis. Ag sacrificial layer was needed total of three printed layers to achieve the critical thickness as required.

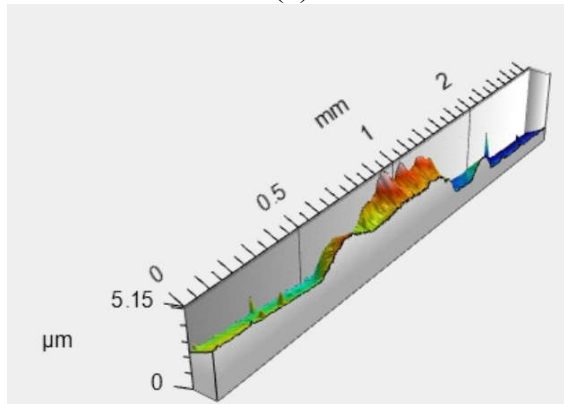


(a)



Parameters	1	Unit
StpHt	2.35	μm

(b)



(c)

Figure 25. Printed sacrificial layer test. (a) on top of PEDOT (b) 2D analysis of the layer for thickness measurement (c) *APEX* 3D analysis for uniformity check

Analysis of Complete Device Before Etching

Fig. 26 (a) shows a complete three-layer printed device, fig. 26 (b) shows the pointed terminal as 1, 2 and 3. In this image, Cantilever beam, transmission line 1 and transmission

line 2 pointed as accordingly 1, 2 and 3. Fig. 26 (c) shows the uniformity of printed layers by *APEX* 3D analysis. The purpose of thickness analysis is to maintain critical thickness of each layer of the device. Later the thickness of the sacrificial is used to calculate the approximate pull-down/actuation voltage. KLA-Tencor scanning has taken in either -Y to +Y direction (fig. 25) or -X to +X direction (fig. 25 and fig. 26).

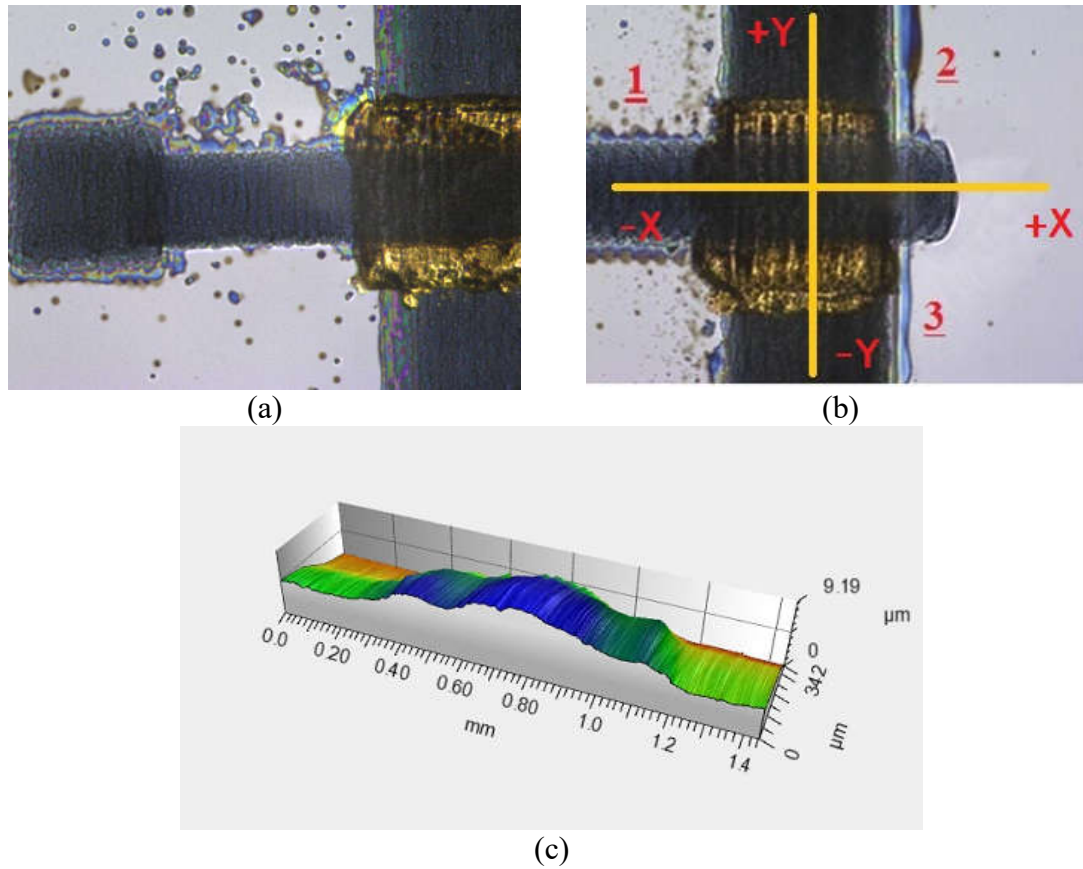


Figure 26. Testing of complete three-layer device. (a) Complete three-layer device (b) three terminal pointed for further data measurement from each terminal (c) uniformity test

Resistance Measurement of the Device Before Etching

Table 11 is the measured resistance between any two of three terminals of the fabricated switch. It is to be noted that, Ag is a very high conductive material ink. Before the removal of sacrificial Ag layer, it is shortening the three terminals of the switch. From the Table 11,

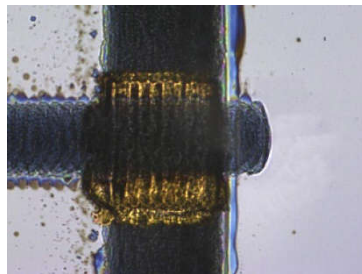
the smaller resistances indicating the short path among these three terminals which is for now should be shorted because of the Ag sacrificial layer.

Table 11. Measured resistance before etching

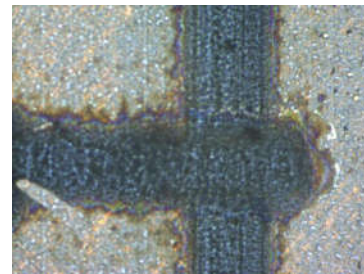
Terminal Points	Resistances (Ω)
1-2	387 ~ 430
1-3	300 ~ 330
2-3	700 ~ 1000

Etching of Ag Sacrificial Layer

Previously developed acid solution is used for etching. Fig. 27 (a) and fig. 27 (b) shows a complete MEMS switch before and after etching. After a total of about 15 minutes of etching, it is evident from the fig. 27 (b) that the Ag sacrificial layer is completely gone. At this moment, it is necessary to measure the resistances again in between two same terminals as previously measured before etching. These resistance values indicate whether the performance of the switch was up to the mark for testing the next step.



(a)



(b)

Figure 27. Device testing before and after etching. (a) before etching (b) after etching

Resistance Measurement of the Device After Etching

Table 12 shows the resistances between any two of three terminals of the MEMS switch after etching the Ag sacrificial layer. These values of the resistances indicate whether the membrane is completely released or not. According to the original design, after the removal

of the sacrificial layer, there should not be any physical contact among three terminals. So theoretically, the resistances in between terminals should be very high after removing sacrificial layer. High resistance value between every two terminals in Table XII is one of the proof that membrane has been released successfully. Another way to prove a successful membrane release is to compare the thickness measurement before and after etching.

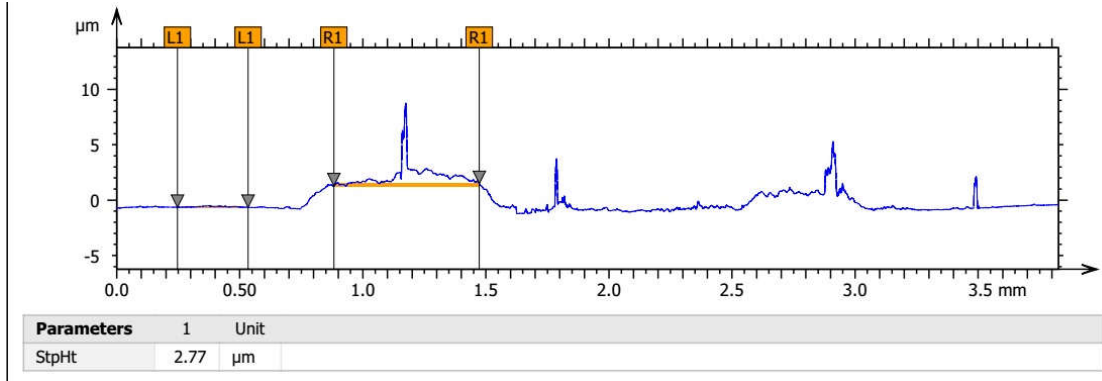
Fig. 27 shows the comparison of thickness before and after etching. Scanning has taken +X to -X direction (fig. 27 (b)). It is seen in fig. 27 (a) that, the thickness of the sacrificial layer region was $2.77\mu\text{m}$ before etching and fig. 27 (b) shows the thickness measurement of the same region after etching which is $2.45\mu\text{m}$. After removal of the sacrificial layer if the cantilever drops off automatically then the thickness would be much less than this value as wouldn't be any air gap between cantilever and transmission lines.

Table 12. Measured resistance after etching

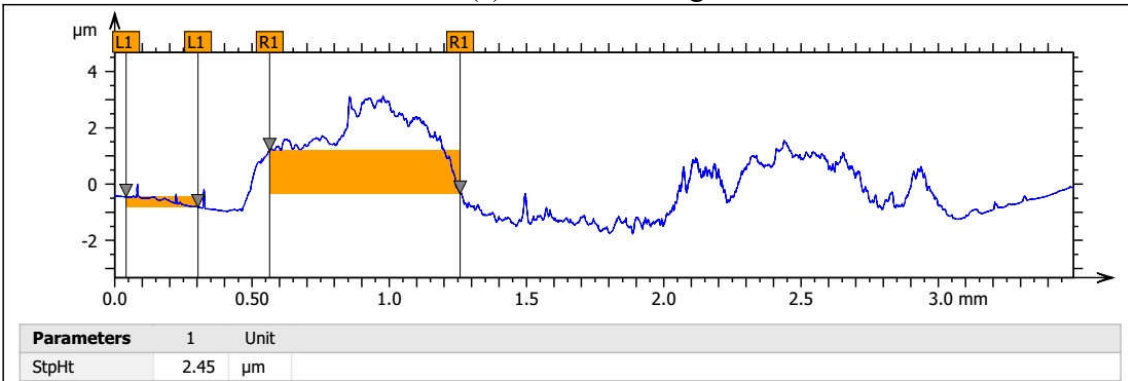
Terminal Points	Resistances (M Ω)
1-2	0.2 ~ 0.3
1-3	0.15 ~ 0.2
2-3	0.45 ~ 0.5

Thickness Comparison Before and After Etching

Fig. 28 shows the 2D thickness comparison of cantilever portion before and after etching sacrificial layer. It is evident that, before etching the thickness was $2.77\mu\text{m}$ and etching it is $2.45\mu\text{m}$. Although cantilever lifted down a little bit, but there are still some air gap between cantilever and transmission lines as the measured resistance is very high in between any two terminals.



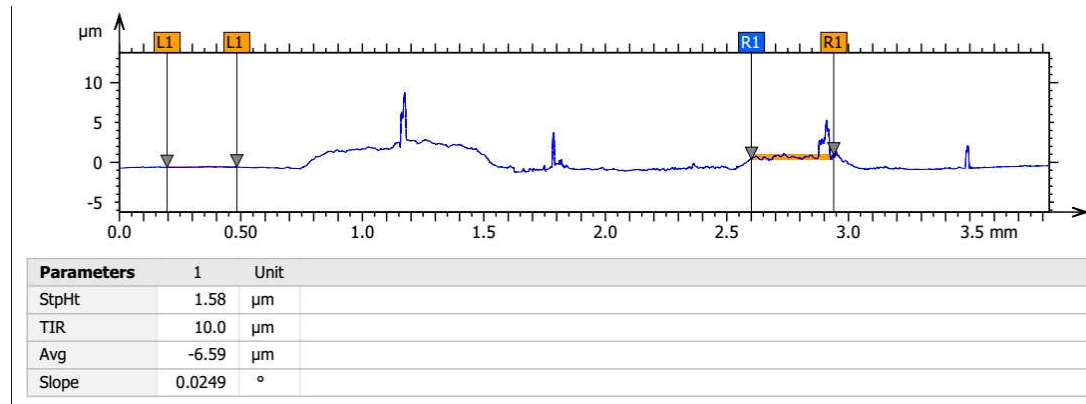
(a) Before etching



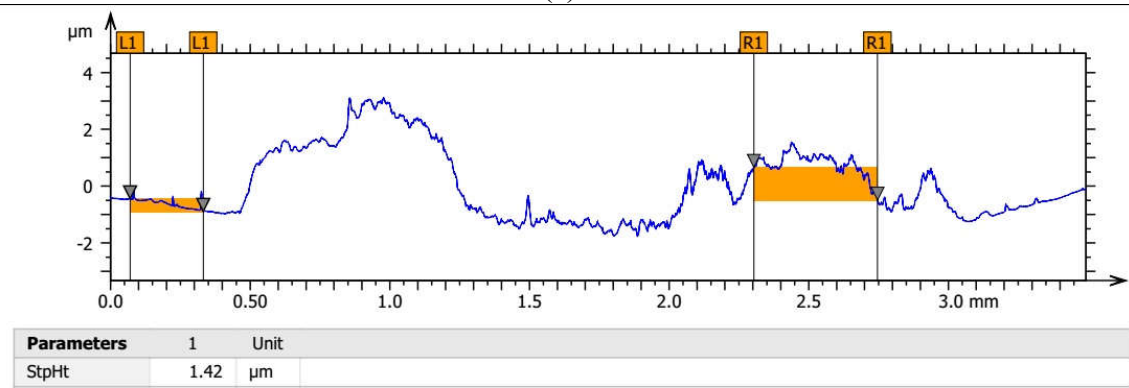
(b) After etching

Figure 28. Thickness comparison after etching

Additionally, fig. 29 shows the comparison of 2D thickness in cantilever anchor region. These two thicknesses are also almost same for before and after etching, which proves that the cantilever was still hanging with some air gap in between cantilever and transmission lines.



(a)



(b)

Figure 29. Thickness comparison in anchor region

MEMS Switch Testing: DC Performance Analysis

Two different connection schemes are used to analyze the dc performance analysis of the switch. Fig. 30 (a) shows the schematic diagram of connection 1. With this type of connection, the input voltage is applied between the cantilever and transmission line 1 and output signal is taken using an ammeter in between the cantilever and transmission line 2. Fig. 30 (b) shows the schematic diagram of connection type 2. In this type of connection, the input voltage is applied between the cantilever and transmission line 2 and output signal is taken from ammeter in between the cantilever and transmission line 1. The reason behind this types of connection is application requirement (i.e. phased array antenna application). The application for this MEMS switch required that, the input signal will be applied in one

side of transmission line and output will be collected from other side when the switch is turned-on.

The input signal was applied by external power supply (Model: GPS-3303) and the output was measured by ammeter option of a multimeter (Model: HP 34401 A)

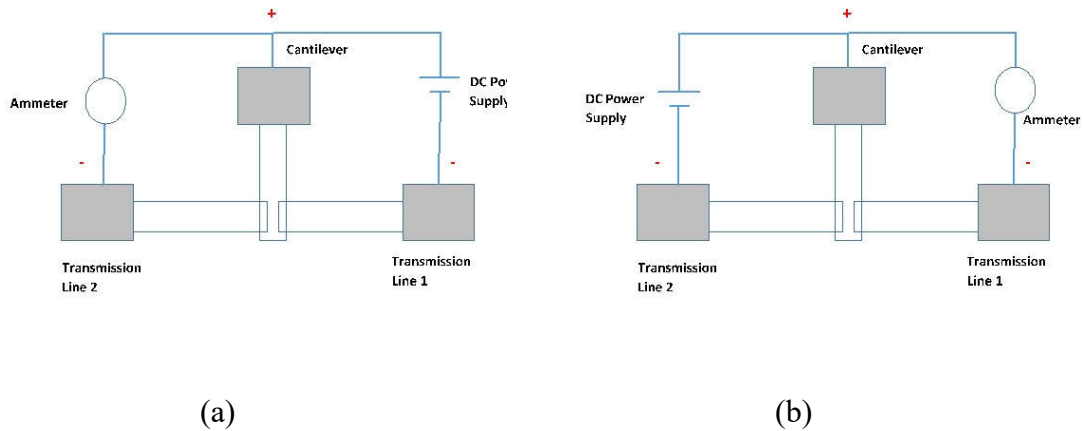


Figure 30. Two different types of connection for device testing

Experimental Results

Table 13 shows the experimental data collected for connection type 1. Collected data for connection type 2 is tabulated in a data table in appendix A. By using the power supply, applied voltage is increased gradually from 0V to 5V which is incremented by 0.2 V. It is seen that, there were very small current (0.0001mA) or no current output till 1.0V. Just after crossing the 1.0V, the device starts conducting with 0.0068mA output current. During the starting of current conduction, the recorded voltage was 1.2V. So, it can be said that, at 1.2 V switch turned on and electrical breakdown happened. The actuation voltage for our fabricated printed MEMS switch is 1.2V.

Table 13. Data table for input voltage and output current for connection type 1

SI No	DC input Voltage between Cantilever and Transmission line 1 (V)	Measured Output Current between Cantilever and transmission line 2 (mA)
1	0	0.0000~0.0001
2	0.2	0.0000~0.0001
3	0.4	0.0000~0.0001
4	0.6	0.0000~0.0001
5	0.8	0.0000~0.0001
6	1.0	0.0000~0.0001
7	1.2	0.0068
8	1.4	0.0107
9	1.6	0.0123
10	1.8	0.0143
11	2.0	0.0155
12	2.2	0.0170
13	2.4	0.0225
14	2.6	0.0300
15	2.8	0.0390
16	3.0	0.0480
17	3.2	0.0581
18	3.4	0.0700
19	3.6	0.0798
20	3.8	0.1070
21	4.0	0.1335
22	4.2	0.1450
23	4.4	0.1670
24	4.6	0.1790
25	4.8	0.1925
26	5.0	0.2195

Fig. 31 presents the plotted data for input voltage vs output current for connection type 1. Measured data vs current is plotted by using MATLAB 2016 version. It is evident from the plot that, it has three different regions such as (0-1.2) V, (1.2 – 5.0) V and beyond

5V. First region is (0-1.1) V where switch doesn't turned-on, second is (1.2-5.0) V is active region for the switch and finally, after 5V, the switch saturates. So, it can be said that, the stand along voltage for the printed switch is 1.2V.

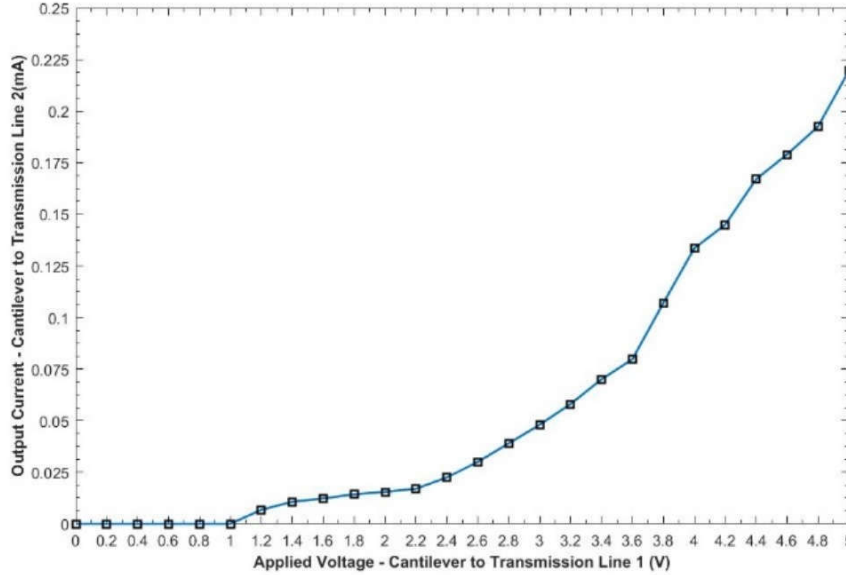


Figure 31. Input voltage vs output current for connection type 1

Calculated Actuation Voltage

Theoretically, the cantilever beam become unstable at $\frac{2}{3}g$ position where g is defined by the height of the beam or the gap between two electrodes [50]. So, the pull-down voltage or actuation voltage is calculated by the following equation [50]. Detail description of this equation is given in appendix B.

$$V_P = V \left(\frac{2g_0}{3} \right) \quad (8)$$

Here, V is the applied voltage.

Table 14 shows some calculated value for actuation voltage in different g_0 value. Air gap of the device is directly proportional to the actuation voltage of the cantilever beam.

So, for low voltage application of this switch it is better to maintain minimum gap between two electrodes.

Table 14. Calculated actuation voltage by considering air gap between electrodes

Air Gap (g_0) in μm	Actuation Voltage (V)
0.5	0.33
1.0	0.67
1.5	1
2.0	1.33
2.5	1.67

The air gap between two electrodes of the printed MEMS switch is $2.45\mu\text{m}$. So, the calculated actuation or pull-down voltage is 1.63V . It is to be noted that, in experiment the pull-down or actuation voltage found 1.2V which is very close to calculated value. Also, the current ON-OFF ration is 68:1 (calculated by the ratio of 0V leakage current and the current during switch tuned-on) with 3.8V of stand along voltage of the printed MEMS switch.

In this chapter, the usages and limitations of the hardware, software and instrumentation were first addressed. After that, step-by-step fabrication with switch characterization has been provided. Finally, dc analysis of the device has been presented. From the dc analysis, it can be concluded that, the experimental result supports the theoretical analysis.

VI. CONCLUSION AND FUTURE WORK

Introduction

This chapter provides a summary, conclusions, and suggestions for future work apart from the thesis. This chapter consists of three sections. The first section of this chapter briefly summarizes each chapter. Major conclusions are presented in the second section and third or final section contains the suggestions for future improvements and the continuation of this thesis.

Summary

This thesis presents the design and fabrication of an electrostatically-actuated inkjet printed MEMS switch. As outlined in Chapter I, it begun with a background study of printing technology, flexible electronics, MEMS switches and other micro switches. This chapter also focused on a historic background study on a normally-open and *SPST* switch cell that operates under certain switching condition. Finally, this chapter ends with the motivation and goals of the thesis and the descriptive summary of the prototype device performance.

In chapter II, the theories of electrical breakdown in narrow air gaps were investigated. Different theoretical breakdown scheme in the narrow air gap was briefly described. This theoretical study establishes the guidelines for future MEMS switch design.

In chapter III, two most important actuation scheme was discussed naming piezoelectric actuation and electrostatic actuation. The operation of the inkjet printed MEMS switch is based on electrostatic actuation; thus, a brief description of this scheme was also given. Finally, the chapter was ended by describing the reason behind choosing the electrostatic actuation scheme.

In chapter IV, step by step fabrication process of printed MEMS switch was discussed. A brief discussion of Fujifilm Dimatix material printer was also given. After that, detail deposition technique and material evaluation process by this printer was illustrated. Finally, this chapter finished by showing step by step fabrication process of first successful printed MEMS switch.

In chapter V, hardware, software and instrumentation usage and limitations were first addressed. After that, step by step fabrication along with characterization of each layer was provided. Finally, DC analysis of the switch was presented. From the DC analysis, it was concluded that, the experimental results support the theoretical analysis.

Conclusions

The primary contribution of this research is to understand the design theories through the experimental characterization of inkjet printed MEMS switch. Chapter IV reaches a conclusive design of inkjet printed MEMS switch. The choice of actuation scheme for this MEMS switch is electrostatics because of the possibility of low power consumption and CMOS compatible materials and processes. Key device specifications such as, actuation voltage (1.2V), stand-off voltage (3.8V), on-state resistance, and ON-OFF ratio (68:1) are evaluated. Theoretically, it is found that, the major disadvantages of large area cantilever beam and a large gap separation needs a significantly high actuation voltage. Based on the test results of DC analysis of the device, on-state electrical breakdown is concluded as 1.2 V, which is the lowest achievable actuation voltage in micron-scale air gaps reported so far. Also the current ON-OFF ratio is 68:1, which is the highest ON-OFF ratio for fully printed MEMS switch reported in literature review so far.

Recommendations for Future Work

This section suggests the directions for further development of the printed MEMS switch and investigates some probable application area. There is some possible device parameter, which could be significantly improved such as off-state performance, stand along voltage, device switching time, power consumption by the switch etc. For the currently fabricated switch, the off-state voltage is only 5V.

Additionally, further Minimization of actuation voltage during turns on the switch could be another point of improvement. Currently fabricated switch has a vast area of application in the phased array antenna field. This switch could be a replacement of the transistor switch if it is possible to minimize the pull-down voltage below 0.5V. Fig. 32 shows the future application of this switch in phased array antenna application. Black arrows in the image shows where the switch will be integrated. This is a 2×2 phased array antenna, bottom 4 antenna elements will be printed by graphene.

[+][Top][2D Wireframe]

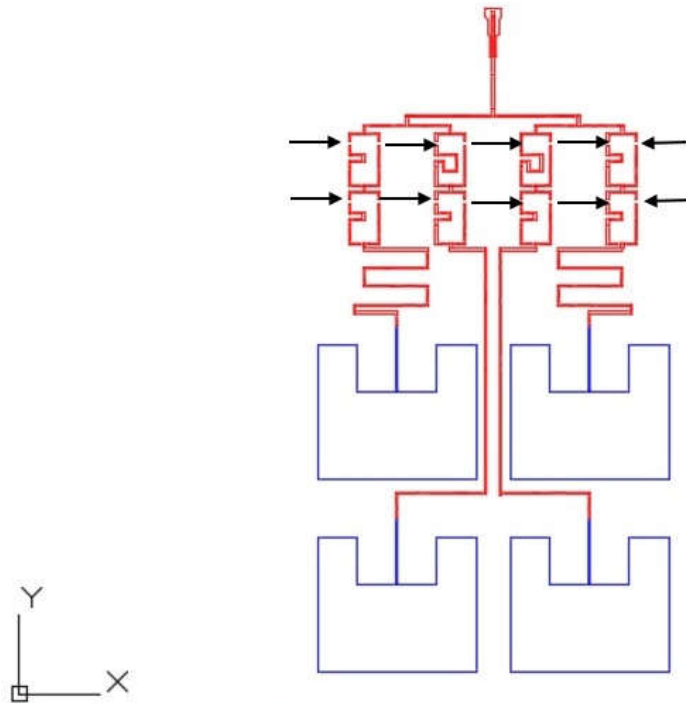


Figure 32. AutoCAD design for 2×2 phased array antenna. Black arrow shows where the printed MEMS switch will be integrated

Miniaturization and accuracy of each printed switch could be improved by adopting another printing technique namely aerosol jet printing. Minimum size that an aerosol jet printer can achieve is 5 μ m both in x-axis and y-axis where inkjet printer has 10 μ m. So, printing resolution can be improved by double with miniaturization of the whole device.

APPENDIX

Appendix A

Table 15. Data table for input voltage and output current for connection type 2

SI No	DC input Voltage between Cantilever and Transmission line 1 (V)	Measured Output Current between Cantilever and transmission line 2 (mA)
1	0	0.0000~0.0001
2	0.2	0.0000~0.0001
3	0.4	0.0000~0.0001
4	0.6	0.0000~0.0001
5	0.8	0.0000~0.0001
6	1.0	0.0000~0.0001
7	1.2	0.0008
8	1.4	0.0030
9	1.6	0.0102
10	1.8	0.0118
11	2.0	0.0208
12	2.2	0.0311
13	2.4	0.0450
14	2.6	0.0679
15	2.8	0.0840
16	3.0	0.0975
17	3.2	0.1184
18	3.4	0.1450
19	3.6	0.1668
20	3.8	0.1763
21	4.0	0.1883
22	4.2	0.1939
23	4.4	0.2194
24	4.6	0.2298
25	4.8	0.2361
26	5.0	0.2368

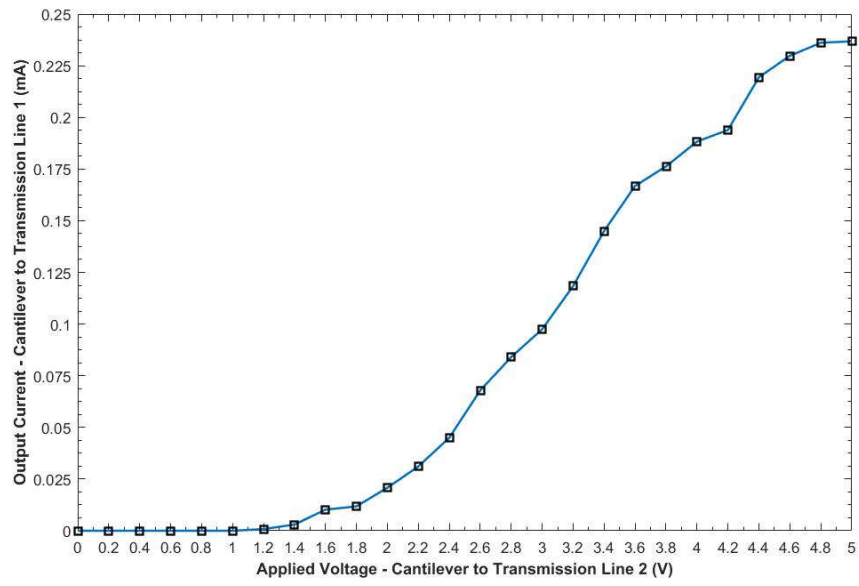


Figure 33. Input voltage vs output current for connection type 2

Appendix B

An electrostatic force is induced on the beam as soon as a voltage is applied between cantilever beam or clamped-clamped beam and the electrode which will be pulled down. Bottom and top electrode behave as a parallel plate capacitor. Thus, to approximate the electrostatic force, pull down electrode is modeled as a parallel-plate capacitor. Suppose the width of beam is B_w and the width of pull down electrode is W , the parallel capacitance is,

$$C = \frac{\epsilon W B_w}{g} \quad (9)$$

Where, g is the height of the beam. And the electrostatic force applied to the beam is

$$F_e = \frac{1}{2} \epsilon \frac{W B_w V^2}{g^2} \quad (10)$$

Now the pull-down voltage is calculated by equating electrostatic force with mechanical restoring force,

$$V = \frac{\sqrt{2K}}{\epsilon W B_w} g^2 (g_0 - g) \quad (11)$$

REFERENCES

- [1] K. Gilleo, *Polymer Thick Film: Today's Emerging Technology for a Clean Environment Tomorrow*. 1996.
- [2] V. Shrotriya, "Organic photovoltaics: Polymer power," *Nature Photonics*, vol. 3, (8), pp. 447-449, 2009.
- [3] M. Hilder, B. Winther-Jensen and N. Clark, "Paper-based, printed zinc–air battery," *J. Power Sources*, vol. 194, (2), pp. 1135-1141, 2009.
- [4] J. Mort and G. Pfister, *Electronic Properties of Polymers*. 1982.
- [5] S. Chang *et al*, "Multicolor organic light-emitting diodes processed by hybrid inkjet printing," *Adv Mater*, vol. 11, (9), pp. 734-737, 1999.
- [6] Y. Yoshioka and G. E. Jabbour, "Desktop inkjet printer as a tool to print conducting polymers," *Synth. Met.*, vol. 156, (11), pp. 779-783, 2006.
- [7] T. Sekitani *et al*, "Stretchable active-matrix organic light-emitting diode display using printable elastic conductors," *Nature Materials*, vol. 8, (6), pp. 494-499, 2009.
- [8] R. Möller *et al*, "Electrical DNA-chip-based identification of different species of the genus *Kitasatospora*," *Appl. Microbiol. Biotechnol.*, vol. 77, (5), pp. 1181-1188, 2008.
- [9] J. B. Chang *et al*, "Printable polythiophene gas sensor array for low-cost electronic noses," *J. Appl. Phys.*, vol. 100, (1), pp. 014506, 2006.
- [10] V. Subramanian *et al*, "Progress toward development of all-printed RFID tags: materials, processes, and devices," *Proc IEEE*, vol. 93, (7), pp. 1330-1338, 2005.
- [11] N. D. Sankir, *Flexible Electronics: Materials and Device Fabrication*, 2005.

- [12] D. T. K. Pham, *Carbon Nanotube Thin Film Transistor on Flexible Substrate and its Applications as Switches in a Phase Shifter for a Flexible Phased-Array Antenna*, 2010.
- [13] J. Perelaer *et al*, "Printed electronics: the challenges involved in printing devices, interconnects, and contacts based on inorganic materials," *Journal of Materials Chemistry*, vol. 20, (39), pp. 8446-8453, 2010.
- [14] D. Hohnholz and A. G. MacDiarmid, "Line patterning of conducting polymers: New horizons for inexpensive, disposable electronic devices," *Synth. Met.*, vol. 121, (1-3), pp. 1327-1328, 2001.
- [15] R. Maoz, S. R. Cohen and J. Sagiv, "Nanoelectrochemical Patterning of Monolayer Surfaces: Toward Spatially Defined Self-Assembly of Nanostructures," *Adv Mater*, vol. 11, (1), pp. 55-61, 1999.
- [16] A. G. MacDiarmid, "Nobel Lecture: "Synthetic metals": A novel role for organic polymers," *Reviews of Modern Physics*, vol. 73, (3), pp. 701, 2001.
- [17] J. Lu, N. J. Pinto and A. G. MacDiarmid, "Apparent dependence of conductivity of a conducting polymer on an electric field in a field effect transistor configuration," *J. Appl. Phys.*, vol. 92, (10), pp. 6033-6038, 2002.
- [18] H. P. Le, "Progress and trends in ink-jet printing technology," *J Imaging Sci Technol*, vol. 42, (1), pp. 49-62, 1998.
- [19] H. S. Nalwa, *Handbook of Nanostructured Materials and Nanotechnology, Five-Volume Set*. 1999.
- [20] T. Forester, *Microelectronics Revolution*. 1981.
- [21] J. G. Kassakian, M. F. Schlecht and G. C. Verghese, *Principles of Power Electronics*. 2000.

- [22] K. Heumann, *Basic Principles of Power Electronics*. 2012.
- [23] K. Petersen, "Micromechanical membrane switches on silicon," *IBM Journal of Research and Development*, vol. 23, (4), pp. 376-385, 1979.
- [24] P. M. Zavracky, S. Majumder and N. E. McGruer, "Micromechanical switches fabricated using nickel surface micromachining," *J Microelectromech Syst*, vol. 6, (1), pp. 3-9, 1997.
- [25] M. Sakata *et al*, "Micromachined relay which utilizes single crystal silicon electrostatic actuator," in *Micro Electro Mechanical Systems, 1999. MEMS'99. Twelfth IEEE International Conference On*, 1999, .
- [26] J. J. Yao and M. F. Chang, "A surface micromachined miniature switch for telecommunications applications with signal frequencies from DC up to 4 GHz," in *Solid-State Sensors and Actuators, 1995 and Eurosensors IX.. Transducers' 95. the 8th International Conference On*, 1995.
- [27] T. Gomm, L. L. Howell and R. H. Selfridge, "In-plane linear displacement bistable microrelay," *J Micromech Microengineering*, vol. 12, (3), pp. 257, 2002.
- [28] A. Hirata *et al*, "A micromechanical switch as the logic elements for circuits in multi chip module on si (MCM-si)," in *Micro Electro Mechanical Systems, 1999. MEMS'99. Twelfth IEEE International Conference On*, 1999.
- [29] W. P. Taylor, O. Brand and M. G. Allen, "Fully integrated magnetically actuated micromachined relays," *J Microelectromech Syst*, vol. 7, (2), pp. 181-191, 1998.
- [30] J. Oberhammer, *Novel RF MEMS Switch and Packaging Concepts*, 2004.
- [31] J. Wong, *Analysis, Design, Fabrication, and Testing of a MEMS Switch for Power Applications*, 2000.

- [32] F. Paschen, "Ueber die zum Funkenübergang in Luft, Wasserstoff und Kohlensäure bei verschiedenen Drucken erforderliche Potentialdifferenz," *Annalen Der Physik*, vol. 273, (5), pp. 69-96, 1889.
- [33] E. E. Kunhardt and L. H. Luessen, *Electrical Breakdown and Discharges in Gases: Part A Fundamental Processes and Breakdown*. 201389.
- [34] J. Meek and J. Craggs, "Electrical breakdown of gases, Clarendon," 1953.
- [35] S. C. Brown, "Introduction to electrical discharges in gases," 1966.
- [36] J. Townsend, *The Theory of Ionization of Gases by Collision*. 1910.
- [37] W. Hopwood, "The positive streamer mechanism of spark breakdown," *Proceedings of the Physical Society. Section B*, vol. 62, (10), pp. 657, 1949.
- [38] C. Muhlstein and S. Brown, "Reliability and fatigue testing of MEMS," in *Tribology Issues and Opportunities in MEMS*, 1998, .
- [39] P. M. Osterberg and S. D. Senturia, "M-TEST: a test chip for MEMS material property measurement using electrostatically actuated test structures," *J Microelectromech Syst*, vol. 6, (2), pp. 107-118, 1997.
- [40] N. P. Suh, *The Principles of Design*. 1990990.
- [41] (). *Dimatix Materials Printer DMP-2800 Series User Manual*.
- [42] Y. KATO, "Fujifilm Group's Inkjet Printhead and Technology," 13th November, 2013.
- [43] d. pham, "Carbon Nanotube Thin Film Transistor on Flexible Substrate and its Applications as Switches in a Phase Shifter for a Flexible Phased-Array Antenna." , 2010.
- [44] (). *Metalon® Conductive Inks for Printed Electronics*.

- [45] S. Aldrich, "Jetting instructions for ORGACONTM IJ-1005," unpublished, private communication, March 2012.
- [46] (2017). *OXYGEN PLASMA TREATMENT IN A RIE PLASMA CHAMBER*.
- [47] K. Dupont, "*DUPONT™ KAPTON® HN Polyimide Film*" unpublished, private communication, 2016.
- [48] Q. Ma *et al*, "Metal contact reliability of RF MEMS switches," in *MOEMS-MEMS 2007 Micro and Nanofabrication*, 2007.
- [49] G. M. Rebeiz, *RF MEMS: Theory, Design, and Technology*. 2004.
- [50] H. Jaafar, F. L. Nan and N. A. M. Yunus, "Design and simulation of high performance RF MEMS series switch," in *Micro and Nanoelectronics (RSM), 2011 IEEE Regional Symposium On*, 2011.